

Fast gradient method for Low-Rank Matrix Estimation

Hongyi Li · Zhen Peng · Chengwei Pan · Di Zhao.

Received: date / Accepted: date

Abstract Projected gradient descent and its Riemannian variant belong to a typical class of methods for low-rank matrix estimation. This paper proposes a new Nesterov's Accelerated Riemannian Gradient algorithm using efficient orthographic retraction and tangent space projection. The subspace relationship between iterative and extrapolated sequences on the low-rank matrix manifold provides computational convenience. With perturbation analysis of truncated singular value decomposition and two retractions, we systematically analyze the local convergence of gradient algorithms and Nesterov's variants in the Euclidean and Riemannian settings. Theoretically, we estimate the exact rate of local linear convergence under different parameters using the spectral radius in a closed form and give the optimal convergence rate and the corresponding momentum parameter. When the parameter is unknown, the adaptive restart scheme can avoid the oscillation problem caused by high momentum, thus approaching the optimal convergence rate. Extensive numerical experiments confirm the estimations of convergence rate and demonstrate that the proposed algorithm is competitive with first-order methods for matrix completion and matrix sensing.

Keywords Low-rank matrix estimation · Local convergence analysis · Riemannian optimization · Nesterov's accelerated Riemannian gradient · Adaptive restart scheme

1 Introduction

Recently, low-rank matrix estimation, as a fundamental model, has played an irreplaceable role in signal processing and machine learning [9]. Such a model

H. Li, Z. Peng and D. Zhao
LMIB, School of Mathematical Sciences, Beihang University, Beijing 100191, China

C. Pan
Institute of Artificial Intelligence, Beihang University, Beijing 100191, China

aims to recover complete information with a latent low-rank structure from the collected measurements $\mathbf{y} = \mathcal{A}(\mathbf{X}_*)$, which is described as follows:

$$\min_{\mathbf{X}} f(\mathbf{X}) := \|\mathcal{A}(\mathbf{X}) - \mathbf{y}\|_2^2 \quad \text{s.t.} \quad \text{rank}(\mathbf{X}) = r, \quad (1)$$

where $\mathcal{A} : \mathbb{R}^{n_1 \times n_2} \mapsto \mathbb{R}^m$ is a linear operator, which arises in various applications, such as Matrix Completion (MC) and Matrix Sensing (MS). Classical convex relaxation bypasses the computationally intractable nonconvex low-rank constraint by nuclear norm minimization. Nonetheless, the computational and space complexity proportional to the matrix size severely limits the applicability of convex relaxations to large-scale problems. Therefore, the nonconvex optimization of the model (1) attracts more attention from researchers [6]. As a well-known class of low-rank matrix estimation algorithms, projected gradient descent alternates between vanilla gradient descent and low-rank matrix projection [11]. The typical one performs a hard-thresholding operation on singular values, thus termed Iterative Hard Thresholding (IHT) [17]. As these Euclidean methods suffer from a high computational burden associated with truncated Singular Value Decomposition (SVD), growing attention has turned to Riemannian optimization [33]. The fact that the rank of the tangent vector does not exceed $2r$ provides an efficient implementation of truncated SVD [5], which inspires a large class of Riemannian gradient descent (RGrad) algorithms.

Since the Heavy-ball method [30] and Nesterov's Accelerated Gradient (NAG) method [27], the introduction of momentum is one of the conventional ways to overcome the short-sighted issue of the gradient algorithm [23, 39]. Theoretically, the NAG algorithm with optimal parameters can match the lower bound of the first-order optimization algorithm [22]. However, on the one hand, optimal parameters are often challenging in practice. On the other hand, iterative sequence oscillations caused by inappropriate parameters can significantly degrade performance. To address the parameter selection issue, a seminal adaptive restart scheme [28] resets momentum when extrapolation is in the wrong direction. Specifically for MC, Vu et al. [34] accurately estimate local linear convergence of a NAG version of IHT via spectral radius, which has recently been generalized under general constraints [36]. The adaptive restart scheme verifies the optimal asymptotic convergence rate in numerical results. Nevertheless, this Euclidean-based acceleration does not enjoy the advantage of the excellent tools on the low-rank matrix manifold, which motivates us to analyze Nesterov's acceleration from a Riemannian perspective.

In contrast to NAG, Nesterov's Accelerated Riemannian Gradient (NARG) method uses operations between tangent spaces and manifolds to ensure that the extrapolation lies on the manifold [3], such as exponential operators, logarithmic operators, and parallel transport. For most matrix manifolds, replacing the exponential operator with matrix factorization-based retraction enables an efficient implementation of NARG [12], for instance, sparse principal component analysis on the Stiefel manifold [15]. The intractable difficulty of NARG is that the inverse of the retraction usually does not have a closed-form expression, requiring an iterative algorithm to solve. In particular, there is little

work on the acceleration of the low-rank matrix manifold because the inverse of projection retraction may not be uniquely defined [2].

Fortunately, although uncommon, orthographic retraction and its inverse admit simple and closed representations [1, 2]. In this paper, we combine NAG and RGrad to develop a novel NARG method for low-rank matrix estimation. To our knowledge, it is the first algorithm that uses orthographic retraction to establish subspace relations between iterative and extrapolated sequences. The overall comparison is shown in Fig. 1. Owing to momentum on the low-rank matrix manifold, NARG has the same computational complexity as RGrad [40, 41], with an advantage in convergence. Based on the efficient implementation of orthographic retraction, the computational complexity of NARG is lower than that of NAG.

Our contributions can be summarized into three folds. 1) We firstly present a first-order perturbation analysis of the retractions, which provides a recursive representation of the iterative error. 2) By analyzing the relation of the spectral radius of the iterative matrix w.r.t. the parameters, we accurately estimate the linear convergence rate of all the algorithms in Fig. 1. 3) The convergence rate of NRAG+R, which uses the *Adaptive Restart Scheme*, can match the theoretical optimal spectral radius.

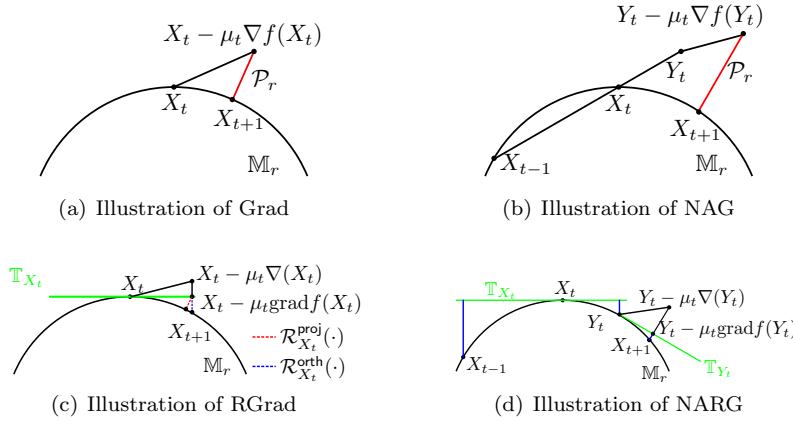


Fig. 1 The overall comparison: the traditional and accelerated methods are compared horizontally, and the Euclidean and Riemannian methods are compared vertically.

For the convenience of readers, we compare representable algorithms for convergence and computational cost in Table 1. The IHT algorithm uses a constant stepsize, and the others use the exact line search. All algorithms exhibit local linear convergence when the condition (8) holds. In a nutshell, the results of NARG+R are dominant in both respects, which will be verified in subsequent experiments.

Table 1 Complexity comparisons between gradient algorithms and Nesterov’s variants in the Euclidean and Riemannian settings.

Algorithm	Geometry	Local Linear Convergence Rate	Dominant per-iteration computational complexity
IHT	Euclidean	$\max(1 - \mu_t \lambda_{\min}, \mu_t \lambda_{\max} - 1) \geq \frac{\kappa-1}{\kappa+1}$	$\mathcal{O}(n^3)$
Grad	Euclidean	$\sqrt{1 - \frac{\tilde{\mu}^2 \lambda_{\max} \lambda_{\min}}{\tilde{\mu}(\lambda_{\max} + \lambda_{\min}) - 1}} \leq \frac{\kappa-1}{\kappa+1}$	$\mathcal{O}(n^3)$
NAG	Euclidean	$\sqrt{\eta_t (1 - \frac{4\lambda_{\min}}{\lambda_{\min} + 3\lambda_{\max}})}$	$\mathcal{O}(n^3)$
RGrad	Riemannian	$\sqrt{1 - \frac{\tilde{\mu}^2 \lambda_{\max} \lambda_{\min}}{\tilde{\mu}(\lambda_{\max} + \lambda_{\min}) - 1}} \leq \frac{\kappa-1}{\kappa+1}$	$\mathcal{O}(n^2 r)$
NARG	Riemannian	$\sqrt{\eta_t (1 - \frac{4\lambda_{\min}}{\lambda_{\min} + 3\lambda_{\max}})}$	$\mathcal{O}(n^2 r)$
NARG+R	Riemannian	$1 - \sqrt{\frac{4\lambda_{\min}}{\lambda_{\min} + 3\lambda_{\max}}} \approx 1 - \sqrt{\frac{1}{\kappa}}$	$\mathcal{O}(n^2 r)$

Parameters: $n = \min(n_1, n_2)$, Gradient stepsize μ_t , Momentum parameter η_t , $\tilde{\mu} = \frac{\|\nabla_{\mathcal{R}} f(\mathbf{X}_t)\|_F^2}{\|\mathbf{A}(\nabla_{\mathcal{R}} f(\mathbf{X}_t))\|_2^2}$

1.1 Notation and Organization

Throughout the paper, vectors are denoted by lowercase letters (e.g., \mathbf{x}), matrices by uppercase letters (e.g., \mathbf{X}), operators by calligraphic letters (e.g., \mathcal{P}), and set of matrices by double-stroke letters (e.g., $\mathbb{R}^{n_1 \times n_2}$). We utilize \mathbf{I}_n as the n -by- n identity matrix and abbreviate as \mathbf{I} without size if the context is clear. Let $\mathbb{O}^{p,r} = \{\mathbf{U} \in \mathbb{R}^{p \times r} : \mathbf{U}^\top \mathbf{U} = \mathbf{I}_r\}$ represent a set of matrices with orthogonal columns. For $\mathbf{U} \in \mathbb{O}^{p,r}$, $\mathbf{U}_\perp \in \mathbb{O}^{p,p-r}$ and $P_{\mathbf{U}} = \mathbf{U}\mathbf{U}^\top$ respectively denote its orthonormal complement and projection matrix. We use $P_{\mathbf{U}}^\perp := P_{\mathbf{U}_\perp} = \mathbf{I} - P_{\mathbf{U}}$ to represent the projection matrix onto perpendicular subspace. Let $\mathbb{M}_r = \{\mathbf{X} \in \mathbb{R}^{n_1 \times n_2} | \text{rank}(\mathbf{X}) = r\}$ be the set of matrices with fixed rank r , which is the smooth submanifold embedded in $\mathbb{R}^{n_1 \times n_2}$. Given $\mathbf{X} \in \mathbb{M}_r$, $\mathbb{T}_{\mathbf{X}}\mathbb{M}_r$ and $\mathbb{T}_{\mathbf{X}}^\perp\mathbb{M}_r$ stand for the tangent space and normal space at \mathbf{X} . We denote $\mathcal{P}_{\mathbb{S}}$ as the projection operator to the set \mathbb{S} . Let the full SVD of n_1 -by- n_2 matrix \mathbf{Y} with $\text{rank}(\mathbf{Y}) = n := \min(n_1, n_2)$ be $\mathbf{Y} = \mathbf{U}_{\mathbf{Y}} \boldsymbol{\Sigma}_{\mathbf{Y}} \mathbf{V}_{\mathbf{Y}}^\top$, where $\mathbf{U}_{\mathbf{Y}} \in \mathbb{O}^{n_1,n}$, $\mathbf{V}_{\mathbf{Y}} \in \mathbb{O}^{n_2,n}$ and $\boldsymbol{\Sigma}_{\mathbf{Y}} = \text{diag}(\sigma_1, \dots, \sigma_n)$ is diagonal matrix with descending order. The projection of \mathbf{Y} to \mathbb{M}_r (a.k.a. truncated SVD) is defined as

$$\mathcal{P}_r(\mathbf{Y}) := [\mathbf{U}_{\mathbf{Y}}]_{:,1:r} [\boldsymbol{\Sigma}_{\mathbf{Y}}]_{1:r,1:r} [\mathbf{V}_{\mathbf{Y}}]_{:,1:r}^\top \in \mathbb{M}_r, \quad (2)$$

where $[\cdot]_{1:r,1:c}$ represents a submatrix composed of some rows and columns of subscript indexes, which is consistent with the expression of Matlab. As some common matrix operations, $\|\cdot\|$, $\|\cdot\|_F$, $\text{vec}(\cdot)$ and \otimes denote the spectral norm, Frobenius norm, vectorization and Kronecker product of the matrix, respectively. In the low-rank estimation problem, $\mathbf{E}_t = \mathbf{X}_t - \mathbf{X}_\star$ represents the residual between the estimate at the t -th iteration and the optimal solution.

The organization of this paper is as follows. The local asymptotic convergence analysis of algorithm Grad with constant stepsize and the exact line search are presented in Sect. 2. Sect. 3 discusses the convergence analysis of NAG. In Sect. 4, we establish the Riemannian versions of Grad and NAG, coined RGrad and NARG, and adopt an adaptive restart scheme to improve the convergence rate of NARG heuristically in Sect. 5. Sect. 6 illustrates the

effectiveness of NARG by numerical studies. Sect. 7 summarizes our work, followed by the proofs in the Appendix.

2 Local convergence of Grad Algorithm

For low-rank matrix estimation such as MS and MC, this section gives a unified representation of the gradient descent algorithm. With the perturbation analysis of truncated SVD, we derive the convergence analysis by the spectral radius of the iterative matrix.

2.1 Vectorization of the gradient

Low-rank matrix estimation is usually a type of least-squares problem (1) with the fixed-rank constraint, and its gradient can be written as

$$\nabla f(\mathbf{X}_t) = \mathcal{A}^*(\mathcal{A}(\mathbf{X}_t - \mathbf{X}_*)) = \mathcal{A}^*(\mathcal{A}(\mathbf{E}_t)),$$

where \mathcal{A}^* is the adjoint operator of the linear operator \mathcal{A} . The vectorization of the gradient and residual matrix satisfies the following linear relationship

$$\text{vec}(\nabla f(\mathbf{X}_t)) = \Theta \text{vec}(\mathbf{E}_t) = \Theta \mathbf{e}_t, \quad (3)$$

where Θ is related to the specific estimation task. Subsequently, we take MC and MS as examples to introduce how to construct the matrix Θ .

MS: The linear measurement operator in MS $\mathcal{A} : \mathbb{R}^{n_1 \times n_2} \mapsto \mathbb{R}^m$ is defined as follows:

$$\mathcal{A}(\mathbf{X}) = [\langle \mathbf{A}_i, \mathbf{X} \rangle]_{1 \leq i \leq m} \in \mathbb{R}^m,$$

where $\{\mathbf{A}_i \in \mathbb{R}^{n_1 \times n_2}\}_{i=1}^m$ is the known matrix set, and its adjoint operator $\mathcal{A}^* : \mathbb{R}^m \mapsto \mathbb{R}^{n_1 \times n_2}$ is defined as $\mathcal{A}^*(\mathbf{y}) = \sum_{i=1}^m \mathbf{y}_i \mathbf{A}_i$. By vectorization, we have

$$\text{vec}(\mathcal{A}^*(\mathcal{A}(\mathbf{E}_t))) = \sum_i [\text{vec}(\mathbf{A}_i)^\top \otimes \text{vec}(\mathbf{A}_i)] \text{vec}(\mathbf{E}_t),$$

thus, the matrix Θ in MS is expressed as follows:

$$\Theta_{\text{MS}} = \sum_i [\text{vec}(\mathbf{A}_i)^\top \otimes \text{vec}(\mathbf{A}_i)]. \quad (4)$$

MC: The purpose of MC is to complete the entire low-rank matrix \mathbf{X}_* based on partial observations $\mathcal{P}_\Omega(\mathbf{X}_*)$. The corresponding loss function is $f(\mathbf{X}) = \|\mathcal{P}_\Omega(\mathbf{X} - \mathbf{X}_*)\|_F^2$, where the projection \mathcal{P}_Ω to the observation index subset Ω is defined as

$$[\mathcal{P}_\Omega(\mathbf{X})]_{i,j} = \begin{cases} \mathbf{X}_{i,j}, & \text{if } (i,j) \in \Omega, \\ 0, & \text{otherwise.} \end{cases}$$

MC can be regarded as a variant of MS [9], and the measurement matrices $\mathbf{A}_{i,j} \in \mathbb{R}^{n_1 \times n_2}$ are set to

$$\mathbf{A}_{i,j} = \mathbf{e}_i^{n_1} \mathbf{e}_j^{n_2 \top} = \begin{cases} 1, & \text{if } (i,j) \in \Omega, \\ 0, & \text{otherwise.} \end{cases}$$

where $\mathbf{e}_i^{n_1}$ represents the i -th column of the identity matrix \mathbf{I}_{n_1} . Hence, the summation (4) is equal to the following binary diagonal matrix, whose main diagonal elements are $\boldsymbol{\omega} = \text{vec}(\sum_{(i,j) \in \Omega} \mathbf{A}_{i,j}) \in \mathbb{R}^{n_1 n_2}$

$$\boldsymbol{\Theta}_{\text{MC}} = \sum_{(i,j) \in \Omega} [\text{vec}(\mathbf{A}_{i,j})^\top \otimes \text{vec}(\mathbf{A}_{i,j})] = \text{diag}(\boldsymbol{\omega}). \quad (5)$$

We denote the cardinality by $|\Omega|$, i.e., the number of observed elements. The selection matrix $\mathbf{S}_\Omega = (\mathbf{e}_{i_k}^{n_1 n_2}) \in \mathbb{R}^{n_1 n_2 \times |\Omega|}$ is constructed by selecting some columns from the identity matrix whose column indices satisfy $\boldsymbol{\omega}_{i_k} = 1$. On the contrary, let the complementary set $\bar{\Omega}$ be unobserved, then the matrix $\mathbf{S}_{\bar{\Omega}}$ consisting of the remaining columns satisfies

$$\begin{aligned} \mathbf{S}_\Omega^\top \mathbf{S}_\Omega &= \mathbf{I}_{|\Omega|}, \mathbf{S}_{\bar{\Omega}}^\top \mathbf{S}_{\bar{\Omega}} = \mathbf{I}_{n_1 n_2 - |\Omega|}, \\ \mathbf{S}_\Omega \mathbf{S}_\Omega^\top + \mathbf{S}_{\bar{\Omega}} \mathbf{S}_{\bar{\Omega}}^\top &= \mathbf{I}_{n_1 n_2}, \\ \text{vec}(\mathcal{P}_\Omega(\mathbf{X})) &= \mathbf{S}_\Omega \mathbf{S}_\Omega^\top \mathbf{x} = \boldsymbol{\Theta}_{\text{MC}} \mathbf{x}, \\ \text{vec}(\mathcal{P}_{\bar{\Omega}}(\mathbf{X})) &= \mathbf{S}_{\bar{\Omega}} \mathbf{S}_{\bar{\Omega}}^\top \mathbf{x} = (\mathbf{I}_{n_1 n_2} - \boldsymbol{\Theta}_{\text{MC}}) \mathbf{x}. \end{aligned} \quad (6)$$

where $\mathbf{x} = \text{vec}(\mathbf{X})$.

2.2 Grad Algorithm with constant stepsize

The Grad Algorithm (see Algorithm 1), a.k.a IHT [17], is a typical projected gradient method for solving (1). It first performs vanilla gradient descent with a constant stepsize $\mu_t \equiv \mu$, then ensures the low-rank constraint by truncating SVD. The Grad Algorithm is illustrated in Fig. 1(a).

Algorithm 1 Grad Algorithm with constant stepsize

Require: observation data \mathbf{y}_{ob} , rank r , maximum iteration T , constant stepsize μ ,

Initialize: $\mathbf{X}_0 = \mathcal{A}^*(\mathbf{y}_{\text{ob}})$,

for $t = 0, 1, \dots, T-1$ **do**

$\mathbf{X}_{t+1} = \mathcal{P}_r(\mathbf{X}_t - \mu \nabla f(\mathbf{X}_t))$,

end for

Ensure: \mathbf{X}_T .

Qualitative convergence analysis of this algorithm and its variants have been extensively studied, see [9]. However, the accurate estimate of the convergence rate has not been systematically studied. A recent framework [36]

describes the asymptotic linear convergence of projected gradient descent. Inspired by this, we combine the gradient and subspace to construct a recursive equation of vectorized errors, where the spectral norm of the iteration matrix can estimate the local linear convergence of Algorithm 1. It is worth mentioning that this result applies to widespread low-rank models such as MC and MS and can be further extended to manifold versions in Sect. 4.

Local convergence for constrained least squares [36] requires the Lipschitz-continuous differentiability of the projection operator \mathcal{P}_r . As an essential tool, the following lemma allows a first-order approximate expansion of the well-known smooth constraint \mathbb{M}_r .

Lemma 1 (Perturbation Analysis of Truncated SVD [10, 34]) *Let $\mathbf{X} = \mathbf{U}\mathbf{\Sigma}\mathbf{V}^\top$ be SVD of matrix \mathbf{X} with rank r . Assuming that the perturbation matrix \mathbf{N} satisfies $\|\mathbf{N}\|_F < \sigma_r(\mathbf{X})/2$, the first-order perturbation expansion of truncated SVD can be formulated as*

$$\mathcal{P}_r(\mathbf{X} + \mathbf{N}) = \mathbf{X} + \mathbf{N} - P_{\mathbf{U}}^\perp \mathbf{N} P_{\mathbf{V}}^\perp + \mathcal{O}(\|\mathbf{N}\|_F^2). \quad (7)$$

According to the above condition, we roughly judge the region of convergence called the *Basin of Attraction*.

$$\|\mathbf{X}_t - \mathbf{X}_*\|_F \asymp \sigma_r(\mathbf{X}_*). \quad (8)$$

Under Lemma 1, once condition (8) holds, the subsequent iterations converge linearly, which is stated as follows.

Theorem 1 (Convergence for Grad with constant stepsize) *Let λ_{\max} and λ_{\min} correspond to the largest and smallest non-zero eigenvalues of $(\mathbf{I} - P_{\mathbf{V}_*}^\perp \otimes P_{\mathbf{U}_*}^\perp)\mathbf{\Theta}$, respectively. The stepsize μ satisfies $\|\mathcal{I} - \mu\mathbf{A}^*\mathbf{A}\| \leq 1$. And set*

$$\rho = \max(1 - \mu\lambda_{\min}, \mu\lambda_{\max} - 1) \leq 1. \quad (9)$$

When condition (8) holds, Algorithm 1 satisfies

$$\|\mathbf{X}_{t+1} - \mathbf{X}_*\|_F \leq \rho \|\mathbf{X}_t - \mathbf{X}_*\|_F. \quad (10)$$

See Appendix B for proof. When $\mathbf{\Theta}$ and \mathbf{X}_* are fixed, the stepsize μ affects the convergence rate. As shown in (9), we give two special stepsizes,

$$\mu_\dagger := 2/(\lambda_{\max} + \lambda_{\min}) \text{ and } \mu_\ddagger := 2/\lambda_{\max}, \quad (11)$$

corresponding to the optimal convergence rate and upper bound, respectively. Obviously, $\mu_\dagger < \mu_\ddagger$. Furthermore, the closer μ is to μ_\dagger , the faster the convergence. Conversely, $\rho > 1$ holds when $\mu \geq \mu_\ddagger$, which means Algorithm 1 does not converge.

Remark 1 The premise of satisfying condition (8) is the convergence guarantee with proper initialization, which has received extensive investigations; see [5, 6, 9] and references therein. On the one hand, some mild statistical assumptions and optimization properties can provide global convergence guarantees

for first-order algorithms [9], such as the number of samples, restricted isometry property, matrix incoherence, and regularity condition. On the other hand, proper initialization can speed up the process of satisfying the condition (8). Subsequent works also establish guarantees that the iteration sequence satisfies local convergence conditions for spectral initialization [8] and random initialization [7], respectively. It is worth mentioning that although the local convergence radius is different under different model assumptions, they are all equal to $\sigma_r(\mathbf{X}_\star)$ up to a constant, which is the same form as the condition (8).

Remark 2 ($\mu = 1$ for MC) In this case, the iteration can be simplified to

$$\mathbf{X}_{t+1} = \mathcal{P}_{\bar{\Omega}}(\mathcal{P}_r(\mathbf{X}_t)) + \mathbf{X}_{\text{ob}}, \text{ where } \mathbf{X}_{\text{ob}} = \mathcal{P}_{\bar{\Omega}}(\mathbf{X}_\star),$$

And the convergence rate is $\rho = 1 - \lambda_{\min}$, which is consistent with [34, 35], due to $\lambda(\mathbf{S}_{\bar{\Omega}}^\top(P_{\mathbf{V}_\star}^\perp \otimes P_{\mathbf{U}_\star}^\perp)\mathbf{S}_{\bar{\Omega}}) = \sigma^2(\mathbf{S}_{\bar{\Omega}}(\mathbf{V}_\perp \otimes \mathbf{U}_\perp))$.

Remark 3 (*Optimal convergence rate*) When $\mu = \mu_\dagger$, the convergence rate $\rho = 1 - \mu_\dagger \lambda_{\min}$ is theoretically optimal, i.e.,

$$\|\mathbf{X}_t - \mathbf{X}_\star\|_F \leq \left(\frac{\kappa - 1}{\kappa + 1}\right)^t \|\mathbf{X}_0 - \mathbf{X}_\star\|_F.$$

where $\kappa = \lambda_{\max}/\lambda_{\min}$ is the condition number of matrix $(\mathbf{I} - P_{\mathbf{V}_\star}^\perp \otimes P_{\mathbf{U}_\star}^\perp)\boldsymbol{\Theta}$.

Remark 4 (*Relation to general optimization problems*) In fact, for a general α -strongly convex and β -smooth function, the convergence rate of the gradient method with stepsize $\mu = \frac{2}{\alpha + \beta}$ is $\frac{\kappa_f - 1}{\kappa_f + 1}$, where $\kappa_f = \frac{\beta}{\alpha}$ is the condition number of the loss function. Similarly, due to the non-expansiveness of projection, it also holds for a class of closed convex-constrained optimization problems. However, it does not consider the geometric properties of constraints. In contrast, Theorem 1 takes full advantage of subspaces of the low-rank constraint. Particularly, when not restricting low-rank constraint, i.e., $P_{\mathbf{V}_\star}^\perp \otimes P_{\mathbf{U}_\star}^\perp = \mathbf{O}_{n_1 n_2}$, the convergence rate degenerates to $\rho = \frac{\kappa_f - 1}{\kappa_f + 1}$.

However, the optimal stepsize μ_\dagger requires the singular matrix pair $(\mathbf{U}_\star, \mathbf{V}_\star)$ to be known in advance, which is not practical in application. Some heuristic adaptive stepsize approaches, such as Normalized IHT (NIHT) [31], have shown effectiveness in theory and practice, motivating us to estimate the convergence rate of exact line search under the low-rank constraint.

2.3 Grad Algorithm with exact line search

Lemma 1 asserts that the low-rank matrix constraint can be locally transformed into linear constraints in subspace form. Once condition (8) is satisfied, applying orthogonal projection to gradient also achieves the same linear convergence rate

$$\nabla_{\mathcal{R}} f(\mathbf{X}) = P_{\mathbf{U}_\mathbf{X}} \nabla f(\mathbf{X}) + \nabla f(\mathbf{X}) P_{\mathbf{V}_\mathbf{X}} - P_{\mathbf{U}_\mathbf{X}} \nabla f(\mathbf{X}) P_{\mathbf{V}_\mathbf{X}}. \quad (12)$$

Similar to Lemma 1, by the orthogonal relationship of the projection, we get

$$\mathcal{P}_r(\mathbf{X}_t - \mu_t \nabla f(\mathbf{X}_t)) = \mathcal{P}_r(\mathbf{X}_t - \mu_t \nabla_{\mathcal{R}} f(\mathbf{X}_t)) + \mathcal{O}(\|\mathbf{E}_t\|_F^2).$$

In fact, $\nabla_{\mathcal{R}} f(\mathbf{X})$ is the Riemannian gradient, which will be analyzed in Sect. 4. Replacing $\nabla f(\mathbf{X})$ with $\nabla_{\mathcal{R}} f(\mathbf{X})$, we get a first-order approximation

$$\begin{aligned} \mathbf{X}_{t+1} &= \mathcal{P}_r(\mathbf{X}_t - \mu_t \nabla_{\mathcal{R}} f(\mathbf{X}_t)) \\ &\stackrel{(a)}{=} \mathbf{X}_t - \mu_t \nabla_{\mathcal{R}} f(\mathbf{X}_t) - P_{\mathbf{U}_*}^\perp \mathbf{E}_t P_{\mathbf{V}_*}^\perp + \mathcal{O}(\|\mathbf{E}_t\|_F^2) \\ &\stackrel{(b)}{=} \mathbf{X}_t - \mu_t \nabla_{\mathcal{R}} f(\mathbf{X}_t) + \mathcal{O}(\|\mathbf{E}_t\|_F^2) \\ &\stackrel{(c)}{\approx} \mathbf{X}_t - \mu_t \nabla_{\mathcal{R}} f(\mathbf{X}_t), \end{aligned}$$

where (a) is similar to Appendix B and (b) uses Lemma 6. The process (c) approximates the optimization problem with low-rank constraint into an unconstrained quadratic problem based on subspaces. The inner product property of the linear operator \mathcal{A} can convert the loss function (1) into vector form

$$\begin{aligned} f(\mathbf{X}) &= \frac{1}{2} \|\mathcal{A}(\mathbf{X}) - \mathbf{y}\|_2^2 = \frac{1}{2} \|\mathcal{A}(\mathbf{X} - \mathbf{X}_*)\|_2^2 = \frac{1}{2} \langle \mathcal{A}(\mathbf{X} - \mathbf{X}_*), \mathcal{A}(\mathbf{X} - \mathbf{X}_*) \rangle \\ &= \frac{1}{2} \langle \mathbf{X} - \mathbf{X}_*, \mathcal{A}^*(\mathcal{A}(\mathbf{X} - \mathbf{X}_*)) \rangle = \frac{1}{2} (\mathbf{x} - \mathbf{x}_*)^\top \boldsymbol{\Theta} (\mathbf{x} - \mathbf{x}_*). \end{aligned}$$

Exact line search aims to minimize $f(\mathbf{X}_t - \mu \nabla_{\mathcal{R}} f(\mathbf{X}_t))$ w.r.t. μ . By vectorization, the adaptive stepsize corresponds to the following problem

$$\mu_t = \underset{\mu}{\operatorname{argmin}} \frac{1}{2} (\mathbf{x}_t - \mu \nabla_{\mathcal{R}} f(\mathbf{x}_t) - \mathbf{x}_*)^\top \boldsymbol{\Theta} (\mathbf{x}_t - \mu \nabla_{\mathcal{R}} f(\mathbf{x}_t) - \mathbf{x}_*).$$

This problem is quadratic and convex w.r.t. μ , and its explicit solution is easy to obtain by the properties of $\nabla_{\mathcal{R}} f(\mathbf{x}_t)$ and $\boldsymbol{\Theta}$ as

$$\mu_t = \frac{\nabla_{\mathcal{R}} f(\mathbf{x}_t)^\top \nabla_{\mathcal{R}} f(\mathbf{x}_t)}{\nabla_{\mathcal{R}} f(\mathbf{x}_t)^\top \boldsymbol{\Theta} \nabla_{\mathcal{R}} f(\mathbf{x}_t)} = \frac{\|\nabla_{\mathcal{R}} f(\mathbf{X}_t)\|_F^2}{\|\mathcal{A}(\nabla_{\mathcal{R}} f(\mathbf{X}_t))\|_2^2}. \quad (13)$$

The above stepsize is consistent with the Riemannian setting [33]. As mentioned previously, the local landscape of the low-rank matrix estimate is equivalent to a quadratic problem. For the latter, the zigzag trajectory phenomenon is inseparable from the asymptotic property of the following lemma.

Lemma 2 (Exact line search [13, 26, 16]) *For an unconstrained quadratic optimization problem*

$$\min_{\mathbf{x} \in \mathbb{R}^n} f(\mathbf{x}) = \frac{1}{2} (\mathbf{x} - \mathbf{x}_*)^\top \mathbf{Q} (\mathbf{x} - \mathbf{x}_*),$$

the gradient descent algorithm with exact line search is iterated as follows:

$$\mathbf{x}_{t+1} = \mathbf{x}_t - \mu_t \nabla f(\mathbf{x}_t), \text{ where } \mu_t = \frac{\nabla f(\mathbf{x}_t)^\top \nabla f(\mathbf{x}_t)}{\nabla f(\mathbf{x}_t)^\top \mathbf{Q} \nabla f(\mathbf{x}_t)}.$$

Then the stepsize sequence $\{\mu_t\}$ is oscillating and satisfies $(\mu_{2k-1}, \mu_{2k}) \rightarrow (\hat{\mu}, \check{\mu})$ with asymptotic behaviour $\hat{\mu}^{-1} + \check{\mu}^{-1} = \lambda_{\max}(\mathbf{Q}) + \lambda_{\min}(\mathbf{Q})$. Moreover, the function value satisfies

$$f(\mathbf{x}_t) \leq \left(\frac{\kappa_{\mathbf{Q}} - 1}{\kappa_{\mathbf{Q}} + 1} \right)^{2t} f(\mathbf{x}_0), \quad (14)$$

where $\kappa_{\mathbf{Q}} := \lambda_{\max}(\mathbf{Q})/\lambda_{\min}(\mathbf{Q})$ is the condition number of the matrix \mathbf{Q} .

Remark 5 (Convergence for the quadratic problem) The inequality (14) can be proved by Kantorovich's inequality. Let the eigenvectors corresponding to the largest and smallest eigenvalues of the matrix \mathbf{Q} be $\mathbf{v}_1, \mathbf{v}_n$, respectively. Then the equality in (14) holds if and only the gradient $\nabla f(\mathbf{x}_0) = \mathbf{Q}(\mathbf{x}_0 - \mathbf{x}_*)$ at the initial point \mathbf{x}_0 can be expressed as a linear combination $k_1\mathbf{v}_1 + k_n\mathbf{v}_n$ with $|k_1/k_n| = 1$. In this case, it is easy to get $\hat{\mu} = \check{\mu} = 2/(\lambda_{\max}(\mathbf{Q}) + \lambda_{\min}(\mathbf{Q}))$, which indicates that the worst-case convergence of the gradient method with exact line search is equivalent to that based on the optimal constant stepsize. Therefore, $(\frac{\kappa_{\mathbf{Q}}-1}{\kappa_{\mathbf{Q}}+1})^2$ is a rough upper bound for the judgment of the convergence rate. To characterize the convergence rate finely, we substitute the asymptotic property of the stepsize into the spectral radius of $\mathbf{I} - \mu_t\mathbf{Q}$ to obtain

$$\bar{\rho} := \sqrt{\rho(\mathbf{I} - \hat{\mu}\mathbf{Q})\rho(\mathbf{I} - \check{\mu}\mathbf{Q})} \approx \sqrt{1 - \frac{\tilde{\mu}^2 \lambda_{\max}(\mathbf{Q}) \lambda_{\min}(\mathbf{Q})}{\tilde{\mu}(\lambda_{\max}(\mathbf{Q}) + \lambda_{\min}(\mathbf{Q})) - 1}}, \quad (15)$$

where $\tilde{\mu} = \frac{\nabla f(\mathbf{x}_0)^\top \nabla f(\mathbf{x}_0)}{\nabla f(\mathbf{x}_0)^\top \mathbf{Q} \nabla f(\mathbf{x}_0)}$ is related to the initial point \mathbf{x}_0 .

We design the following Algorithm 2 based on the exact line search.

Algorithm 2 Grad Algorithm with exact line search

Require: observation \mathbf{y}_{ob} , rank r , maximum iteration T .

Initialize: $\mathbf{X}_0 = \mathcal{A}^*(\mathbf{y}_{\text{ob}})$.

for $t = 0, 1, \dots, T-1$ **do**

 compute $\nabla_{\mathcal{R}} f(\mathbf{X}_t) = \nabla f(\mathbf{X}_t) - P_{\mathcal{U}_t}^\perp \nabla f(\mathbf{X}_t) P_{\mathcal{V}_t}^\perp$,

 exact line search rule $\mu_t = \frac{\|\nabla_{\mathcal{R}} f(\mathbf{X}_t)\|_F^2}{\|\mathcal{A}(\nabla_{\mathcal{R}} f(\mathbf{X}_t))\|_2^2}$,

$\mathbf{X}_{t+1} = \mathcal{P}_r(\mathbf{X}_t - \mu_t \nabla_{\mathcal{R}} f(\mathbf{X}_t))$,

end for

Ensure: \mathbf{X}_T .

Similar to the asymptotic property of exact line search in Lemma 2, the following proposition uses the spectral radius to estimate the convergence rate of Algorithm 2 accurately.

Proposition 1 (Convergence for Grad with exact line search) *Let λ_{\max} and λ_{\min} correspond to the largest and smallest non-zero eigenvalues of $(\mathbf{I} - P_{\mathcal{V}_*}^\perp \otimes P_{\mathcal{U}_*}^\perp)\Theta$, respectively. The condition number is denoted as $\kappa :=$*

$\lambda_{\max}/\lambda_{\min}$. When condition (8) holds, the function value of Algorithm 2 satisfies

$$f(\mathbf{X}_{t+1}) \leq \left(\frac{\kappa-1}{\kappa+1}\right)^2 f(\mathbf{X}_t).$$

Furthermore, the residual satisfies the following recursion

$$\|\mathbf{X}_{t+1} - \mathbf{X}_*\|_F \leq \sqrt{1 - \frac{\tilde{\mu}^2 \lambda_{\max} \lambda_{\min}}{\tilde{\mu}(\lambda_{\max} + \lambda_{\min}) - 1}} \|\mathbf{X}_t - \mathbf{X}_*\|_F,$$

where $\tilde{\mu} = \frac{\|\nabla_{\mathcal{R}} f(\mathbf{X}_t)\|_F^2}{\|\mathcal{A}(\nabla_{\mathcal{R}} f(\mathbf{X}_t))\|_2^2} \in [\lambda_{\max}^{-1}, \lambda_{\min}^{-1}]$.

See Appendix C for proof. By a simple algebraic inequality, we have

$$\sqrt{1 - \frac{\tilde{\mu}^2 \lambda_{\max} \lambda_{\min}}{\tilde{\mu}(\lambda_{\max} + \lambda_{\min}) - 1}} \leq \frac{\kappa-1}{\kappa+1},$$

which means that the worst convergence rate of exact line search is precisely that of the optimal constant stepsize, see Remarks 3 and 5.

Remark 6 (Related Work) The stepsize we use differs from the classic NIHT [31] in the projection direction. NIHT uses the projection matrix composed of the first r left and right singular vectors as the search restriction direction to improve the correction of singular values, as follows:

$$\mu_t^u := \frac{\|P_{\mathbf{U}_t} \nabla f(\mathbf{X}_t)\|_F^2}{\|\mathcal{A}(P_{\mathbf{U}_t} \nabla f(\mathbf{X}_t))\|_2^2}, \mu_t^v := \frac{\|\nabla f(\mathbf{X}_t) P_{\mathbf{V}_t}\|_F^2}{\|\mathcal{A}(\nabla f(\mathbf{X}_t) P_{\mathbf{V}_t})\|_2^2}, \mu_t^{uv} := \frac{\|P_{\mathbf{U}_t} \nabla f(\mathbf{X}_t) P_{\mathbf{V}_t}\|_F^2}{\|\mathcal{A}(P_{\mathbf{U}_t} \nabla f(\mathbf{X}_t) P_{\mathbf{V}_t})\|_2^2}.$$

In contrast, the projection gradient (12) takes into account all three directions to set the stepsize (13).

3 Local convergence of NAG Algorithm

In this section, we will improve the local linear convergence rate of the Grad algorithm by introducing momentum. As demonstrated in the following iterations, the core of NAG is to use the extrapolated trend generated by momentum to speed up the first-order optimization method

$$\begin{aligned} \mathbf{Y}_{t+1} &= \mathbf{X}_{t+1} + \eta_t (\mathbf{X}_{t+1} - \mathbf{X}_t), \\ \mathbf{X}_{t+1} &= \mathbf{Y}_{t+1} - \mu_t \nabla f(\mathbf{Y}_{t+1}). \end{aligned} \tag{16}$$

This idea is widely used in various fields and has fascinating interpretations, such as variational framework [42], integral quadratic constraint [21]. Similar to [34], we employ this general acceleration technique for low-rank matrix estimation and obtain the following algorithm. An illustration of the NAG is shown in Fig. 1(b).

Algorithm 3 Nesterov's Accelerated Gradient (NAG)**Require:** observation \mathbf{y}_{ob} , rank r , maximum iteration T .Initialize: $\mathbf{X}_{-1} = \mathbf{X}_0 = \mathcal{A}^*(\mathbf{y}_{\text{ob}})$.**for** $t = 0, 1, \dots, T-1$ **do** compute extrapolation: $\mathbf{Y}_t = \mathbf{X}_t + \eta_t(\mathbf{X}_t - \mathbf{X}_{t-1})$ with proper η_t , compute $\nabla_{\mathcal{R}} f(\mathbf{Y}_t) = \nabla f(\mathbf{Y}_t) - P_{\mathcal{U}_t}^\perp \nabla f(\mathbf{Y}_t) P_{\mathcal{V}_t}^\perp$, exact line search rule $\mu_t = \frac{\|\nabla_{\mathcal{R}} f(\mathbf{Y}_t)\|_F^2}{\|\mathcal{A}(\nabla_{\mathcal{R}} f(\mathbf{Y}_t))\|_2^2}$, $\mathbf{X}_{t+1} = \mathcal{P}_r(\mathbf{Y}_t - \mu_t \nabla_{\mathcal{R}} f(\mathbf{Y}_t))$,**end for****Ensure:** \mathbf{X}_T .

We analyze the relationship between the spectral radius of the iterative matrix and (μ_t, η_t) in detail and generalize the convergence analysis in [18] to low-rank matrix estimation as the following theorem.

Theorem 2 (Optimal Convergence Rate of NAG) *Let λ_{\max} and λ_{\min} correspond to the largest and smallest non-zero eigenvalues of $(\mathbf{I} - P_{\mathcal{V}_*}^\perp \otimes P_{\mathcal{U}_*}^\perp)\Theta$, respectively. The parameter pair (μ_t, η_t) represents the stepsize and momentum parameter, where μ_t satisfies $\|\mathcal{I} - \mu_t \mathcal{A}^* \mathcal{A}\| \leq 1$ and $\eta_t \in [0, 1]$. Set $\mathbf{H}(\mu_t) = (\mathbf{I} - P_{\mathcal{V}_*}^\perp \otimes P_{\mathcal{U}_*}^\perp)(\mathbf{I} - \mu_t \Theta)$. Then the vectorization of the residuals $\mathbf{e}_t = \mathbf{x}_t - \mathbf{x}_*$ corresponding to the sequence $\{\mathbf{X}_t\}$ generated by Algorithm 3 satisfies*

$$\begin{pmatrix} \mathbf{e}_{t+1} \\ \mathbf{e}_t \end{pmatrix} = \underbrace{\begin{pmatrix} (1 + \eta_t)\mathbf{H}(\mu_t) - \eta_t\mathbf{H}(\mu_t) & \\ \mathbf{I} & \mathbf{0} \end{pmatrix}}_{\mathbf{T}(\mu_t, \eta_t)} \begin{pmatrix} \mathbf{e}_t \\ \mathbf{e}_{t-1} \end{pmatrix} \quad (17)$$

When condition (8) holds, Algorithm 3 satisfies the following recursion

$$(\|\mathbf{e}_{t+1}\|_2^2 + \|\mathbf{e}_t\|_2^2) \leq \rho(\mathbf{T}(\mu_t, \eta_t))^2 (\|\mathbf{e}_t\|_2^2 + \|\mathbf{e}_{t-1}\|_2^2).$$

When $(\mu_t, \eta_t) \equiv (\mu_b, \eta_b) := (\frac{4}{\lambda_{\min} + 3\lambda_{\max}}, \frac{1 - \sqrt{\mu_b \lambda_{\min}}}{1 + \sqrt{\mu_b \lambda_{\min}}})$, Algorithm 3 achieves the optimal convergence rate, i.e.,

$$\rho_{\text{opt}} = \min_{\mu, \eta} \rho(\mathbf{T}(\mu, \eta)) = 1 - \sqrt{\frac{4\lambda_{\min}}{\lambda_{\min} + 3\lambda_{\max}}}. \quad (18)$$

See Appendix D for proof. The optimal convergence rate matches the lower bounds for first-order optimization algorithms (up to constant), which is consistent with NAG for the quadratic problems [18].

As we all know, the NAG is not a strict descent algorithm, and the momentum parameter can affect its acceleration performance. The acceleration mechanism can be cast as a linear dynamical system [28]. We also calculate the optimal momentum parameter $\eta^-(\mu_t)$ w.r.t. μ_t in Appendix D and partition according to the behavior of iterative oscillations.

- $\eta_t < \eta^-(\mu_t)$: low momentum region, overdamped,
- $\eta_t = \eta^-(\mu_t)$: optimal momentum, critically damped,

– $\eta_t > \eta^-(\mu_t)$: high momentum region, underdamped.

Since the optimal momentum is usually unknown, the parameter monotonically increases from 0 to 1, i.e., $\eta_t : 0 \nearrow 1$. It inevitably leads to performance degradation caused by the underdamped iteration. To avoid the high momentum, the adaptive restart scheme [28] properly resets the parameter when the underdamped occurs, which we will discuss in Sect. 5. Another effective Lazy strategy [25] sets $\eta_t = \frac{t-1}{t+d}$ and demonstrates that the larger the parameter d , the better the algorithm performance of NAG. Since the exact line search outperforms the optimal constant stepsize, the following corollary gives an upper bound of the convergence rate of NAG under the Lazy strategy.

Corollary 1 (Convergence Rate of NAG) *When the momentum parameter $\eta_t = \frac{t-1}{t+d} \geq \eta_b$, the iteration error generated by Algorithm 3 satisfies*

$$\|e_{t+1}\|_2 + \|e_t\|_2 \leq \sqrt{\eta_t(1 - \mu_b \lambda_{\min})}(\|e_t\|_2 + \|e_{t-1}\|_2).$$

The convergence rate of NAG gradually becomes slower under the Lazy strategy, so it does not belong to linear convergence. Once we have the minimum number of iterations t_0 that satisfies condition (8) and the total number of iterations t_n , we can roughly estimate the average convergence rate.

$$\begin{aligned} \bar{\rho}_{\text{NAG}} &= \left(\prod_{t=t_0}^{t_n} \eta_t \right)^{1/(2(t_n-t_0+1))} \sqrt{1 - \mu_b \lambda_{\min}} \\ &= \left(\prod_{i=0}^d \frac{t_0 + i - 1}{t_n + i - 1} \right)^{1/(2(t_n-t_0+1))} \sqrt{1 - \mu_b \lambda_{\min}} \end{aligned} \quad (19)$$

Note that Algorithm 3 needs two SVDs in the update step μ_t and truncated SVD. By changing the order, the following algorithm only needs one SVD, and the convergence is the same as Algorithm 3.

$$\begin{aligned} \mathbf{Y}_t &= \mathcal{P}_r(\mathbf{Z}_t), \\ \mathbf{X}_{t+1} &= \mathbf{Y}_t - \mu_t \nabla_{\mathcal{R}} f(\mathbf{Y}_t), \\ \mathbf{Z}_{t+1} &= \mathbf{X}_{t+1} + \eta_t (\mathbf{X}_{t+1} - \mathbf{X}_t). \end{aligned} \quad (20)$$

However, those Euclidean methods, such as Algorithm 2 and Algorithm 3, still suffer from the high computational cost caused by SVD. To overcome the burden, we use the Riemannian gradient descent algorithm to solve the problem (1).

4 Extension to Riemannian Optimization

In this section, we use the tools of the Riemannian manifold, such as subspace projection and retraction, to reduce the computational cost of algorithms in Sect. 2 and Sect. 3. Further, we combine Nesterov's ideas and low-rank manifold tools to design algorithms with advantages in both time and space.

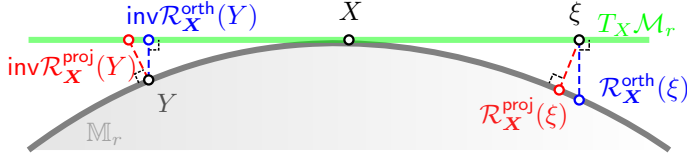


Fig. 2 Geometric comparison between projective retraction and orthographic retraction.

4.1 Preliminaries on the geometry of low-rank matrix manifold

Assume SVD of $\mathbf{X} \in \mathbb{M}_r \subset \mathbb{R}^{n_1 \times n_2}$ is $\mathbf{X} = \mathbf{U}_\mathbf{X} \boldsymbol{\Sigma}_\mathbf{X} \mathbf{V}_\mathbf{X}^\top$. The tangent space $\mathbb{T}_\mathbf{X} \mathbb{M}_r$ can be constructed by the direct sum of the row and column subspaces of \mathbf{X} .

$$\mathbb{T}_\mathbf{X} \mathbb{M}_r = \{\mathbf{U}_\mathbf{X} \mathbf{M} \mathbf{V}_\mathbf{X}^\top + \mathbf{U}_p \mathbf{V}_\mathbf{X}^\top + \mathbf{U}_\mathbf{X} \mathbf{V}_p^\top : \mathbf{U}_p^\top \mathbf{U}_\mathbf{X} = \mathbf{V}_p^\top \mathbf{V}_\mathbf{X} = \mathbf{0}_{r \times r}\}. \quad (21)$$

where $\mathbf{M} \in \mathbb{R}^{r \times r}$, $\mathbf{U}_p \in \mathbb{R}^{n_1 \times r}$, $\mathbf{V}_p \in \mathbb{R}^{n_2 \times r}$. The projection of any point $\mathbf{Z} \in \mathbb{R}^{n_1 \times n_2}$ to $\mathbb{T}_\mathbf{X} \mathbb{M}_r$ is

$$\mathcal{P}_{\mathbb{T}_\mathbf{X} \mathbb{M}_r}(\mathbf{Z}) = P_{\mathbf{U}_\mathbf{X}} \mathbf{Z} + \mathbf{Z} P_{\mathbf{V}_\mathbf{X}} - P_{\mathbf{U}_\mathbf{X}} \mathbf{Z} P_{\mathbf{V}_\mathbf{X}}. \quad (22)$$

Optimization on the manifold: For a given differentiable function $f(\mathbf{X})$, the general step for solving the optimization problem $\min_{\mathbf{X} \in \mathbb{M}_r} f(\mathbf{X})$ on the manifold \mathbb{M}_r is as follows

$$\mathbf{X}_{t+1} = \mathcal{R}_{\mathbf{X}_t}(-\eta_t \text{grad} f(\mathbf{X}_t)), \quad (23)$$

where $\text{grad} f(\mathbf{X}_t) = \mathcal{P}_{\mathbb{T}_{\mathbf{X}_t} \mathbb{M}_r} \nabla f(\mathbf{X}_t)$ represents the Riemannian gradient, which is obtained by projecting the Euclidean gradient to the tangent space. A critical step is to pull the result from the tangent space back to the manifold through the retraction, denoted as $\mathcal{R}_\mathbf{X}(\cdot) : \mathbb{T}_\mathbf{X} \mathbb{M}_r \rightarrow \mathbb{M}_r$. We will briefly describe two common retractions: Projective retraction and Orthographic retraction. In addition, we will introduce the inverse retraction, denoted $\text{inv} \mathcal{R}_\mathbf{X}(\cdot) : \mathbb{M}_r \rightarrow \mathbb{T}_\mathbf{X} \mathbb{M}_r$. These concepts are visually described in Fig. 2.

Projective retraction: For any tangent vector $\boldsymbol{\delta} \in \mathbb{T}_\mathbf{X} \mathbb{M}_r$, the approximation problem corresponding to projective retraction can be solved by truncation SVD, i.e., $\mathcal{R}_\mathbf{X}^{\text{proj}}(\boldsymbol{\delta}) = \mathcal{P}_r(\mathbf{X} + \boldsymbol{\delta})$. The computational cost on truncation SVD is $\mathcal{O}(n^3)$, where $n = \min(n_1, n_2)$. Considering the representation of the tangent vector in (21), we can rewrite the matrix $\mathbf{X} + \boldsymbol{\delta}$ as a block matrix

$$\mathbf{X} + \boldsymbol{\delta} = [\mathbf{U}_\mathbf{X} \ \mathbf{U}_p] \begin{bmatrix} \boldsymbol{\Sigma}_\mathbf{X} + \mathbf{M} & \mathbf{I}_r \\ \mathbf{I}_r & \mathbf{0} \end{bmatrix} [\mathbf{V}_\mathbf{X} \ \mathbf{V}_p]^\top. \quad (24)$$

Obviously, $\text{rank}(\mathbf{X} + \boldsymbol{\delta}) \leq 2r$. The original SVD of (24) can be equivalently converted into two QR factorizations, one $2r \times 2r$ SVD and a few matrix multiplications [33, 4, 38], with a total computational cost of $\mathcal{O}(n^2 r + n^2 +$

$nr^2 + r^3$), which greatly reduces the complexity when $r \ll n$. The inverse projective retraction satisfies the following form.

$$\text{inv}\mathcal{R}_{\mathbf{X}}^{\text{proj}}(\mathbf{X} + \boldsymbol{\delta}) = (\mathbf{X} + \mathbb{T}_{\mathbf{X}}\mathbb{M}_r) \cap (\mathbf{X} + \boldsymbol{\delta} + \mathbb{T}_{\mathbf{X} + \boldsymbol{\delta}}^{\perp}\mathbb{M}_r) - \mathbf{X}.$$

However, the inverse relies on tangent and normal spaces and does not have a closed-form representation.

Orthographic retraction: For any tangent vector $\boldsymbol{\delta} \in \mathbb{T}_{\mathbf{X}}\mathbb{M}_r$, the orthographic retraction is defined as the closest point to $\mathbf{X} + \boldsymbol{\delta}$ in the vertical direction of the tangent space, i.e., $\mathbf{X} + \boldsymbol{\delta} + \mathbb{T}_{\mathbf{X}}^{\perp}\mathbb{M}_r \cap \mathbb{M}_r$, which has an explicit solution [44]

$$\mathcal{R}_{\mathbf{X}}^{\text{orth}}(\boldsymbol{\delta}) = (\mathbf{X} + \boldsymbol{\delta})\mathbf{V}_{\mathbf{X}}[\mathbf{U}_{\mathbf{X}}^{\top}(\mathbf{X} + \boldsymbol{\delta})\mathbf{V}_{\mathbf{X}}]^{-1}\mathbf{U}_{\mathbf{X}}^{\top}(\mathbf{X} + \boldsymbol{\delta}). \quad (25)$$

The above formula only involves multiple matrix multiplications and a matrix inverse of $r \times r$, so it is efficient. We are more concerned about constructing the tangent space of the next iteration from the current tangent space through SVD. As suggested in [2], the original SVD of (25) can also be equivalently converted into two QR factorizations and a $r \times r$ SVD. Specifically, we calculate $(\mathbf{X} + \boldsymbol{\delta})\mathbf{V}_{\mathbf{X}} = \mathbf{Q}_1\mathbf{R}_1$, $(\mathbf{X} + \boldsymbol{\delta})^{\top}\mathbf{U}_{\mathbf{X}} = \mathbf{Q}_2\mathbf{R}_2$ and $\mathbf{R}_1[\mathbf{U}_{\mathbf{X}}^{\top}(\mathbf{X} + \boldsymbol{\delta})\mathbf{V}_{\mathbf{X}}]^{-1}\mathbf{R}_2^{\top} = \mathbf{U}_b\boldsymbol{\Sigma}_b\mathbf{V}_b^{\top}$. Then orthographic retraction can be expressed as follows with SVD form

$$\mathcal{R}_{\mathbf{X}}^{\text{orth}}(\boldsymbol{\delta}) = \underbrace{(\mathbf{Q}_1\mathbf{U}_b)}_{\mathbf{U}_+} \underbrace{\boldsymbol{\Sigma}_b}_{\boldsymbol{\Sigma}_+} \underbrace{(\mathbf{Q}_2\mathbf{V}_b)^{\top}}_{\mathbf{V}_+}. \quad (26)$$

The computational cost involved is consistent with the projective retraction. Due to the orthogonal relationship to the tangent space, the inverse orthographic retraction is a simple projection to tangent space, i.e., $\text{inv}\mathcal{R}_{\mathbf{X}}^{\text{orth}}(\mathbf{Y}) = \mathcal{P}_{\mathbb{T}_{\mathbf{X}}\mathbb{M}_r}(\mathbf{Y} - \mathbf{X})$.

4.2 RGrad Algorithm with exact line search

Referring to [40, 41, 44], we reformulate the RGrad under exact line search, see Algorithm 4. As shown in Fig. 1(c), the retraction $\mathcal{R}_{\mathbf{X}}$ can be chosen one of the projected $\mathcal{R}_{\mathbf{X}}^{\text{proj}}$ and the orthogonal $\mathcal{R}_{\mathbf{X}}^{\text{orth}}$.

Algorithm 4 Riemannian gradient descent (RGrad)

Require: observation \mathbf{y}_{ob} , rank r , maximum iteration T .

Initialize: $\mathbf{X}_0 = \mathcal{A}^*(\mathbf{y}_{\text{ob}})$

for $t = 0, 1, \dots, T - 1$ **do**

 exact line search rule $\mu_t = \frac{\|\text{grad } f(\mathbf{X}_t)\|_F^2}{\|\mathcal{A}(\text{grad } f(\mathbf{X}_t))\|_2^2}$

$\mathbf{X}_{t+1} = \mathcal{R}_{\mathbf{X}_t}(-\mu_t \text{grad } f(\mathbf{X}_t))$

end for

Ensure: \mathbf{X}_T .

Thanks to the efficient implementation of retraction, the computational complexity of RGrad is lower than that of Grad. In the following lemma, we introduce the perturbation analysis of retractions, which can reflect retractions and truncated SVD have the same first-order perturbation expansion.

Lemma 3 (Perturbation analysis of retractions) *Let SVD of the matrix $\mathbf{X} \in \mathbb{M}_r$ be $\mathbf{X} = \mathbf{U}_\mathbf{X} \boldsymbol{\Sigma}_\mathbf{X} \mathbf{V}_\mathbf{X}^\top$. Assuming that the perturbation matrix \mathbf{N} satisfies $\|\mathbf{N}\|_F < \sigma_r(\mathbf{X})/2$, the first-order perturbation expansion of retractions satisfies*

$$\begin{aligned} \mathcal{R}_\mathbf{X}^{\text{proj}}(\mathbf{N}) &= \mathcal{P}_{\mathbb{T}_\mathbf{X}}(\mathbf{X} + \mathbf{N}) + \mathcal{O}(\|\mathbf{N}\|_F^2), \\ \mathcal{R}_\mathbf{X}^{\text{orth}}(\mathbf{N}) &= \mathcal{P}_{\mathbb{T}_\mathbf{X}}(\mathbf{X} + \mathbf{N}) + \mathcal{O}(\|\mathbf{N}\|_F^2). \end{aligned} \quad (27)$$

See Appendix E.1 for proof. The iterative matrix derived by RGrad is consistent with Grad in Appendix E.2, which means the same convergence rate.

4.3 Nesterov's Accelerated Riemannian Gradient

From a manifold point of view, the extrapolation along the geodesic involves the exponential and the logarithmic maps [43, 19]. Fortunately, these maps on the low-rank matrix manifold can often be replaced by first-order approximation, the retraction [33, 12]. Compared with projective retraction, orthographic retraction has an explicit inverse, i.e., projection $\mathcal{P}_{\mathbb{T}_\mathbf{X}\mathbb{M}_r}$. Next, we establish the NARG Algorithm based on orthographic retraction.

Algorithm 5 Nesterov's Accelerated Riemannian Gradient (NARG)

Require: observation \mathbf{y}_{ob} , rank r , maximum iteration T .

Initialize: $\mathbf{X}_{-1} = \mathbf{X}_0 = \mathcal{A}^*(\mathbf{y}_{\text{ob}})$.

for $t = 0, 1, \dots, T - 1$ **do**

 choose proper η_t and set extrapolation: $\mathbf{Y}_t = \mathcal{R}_{\mathbf{X}_t}^{\text{orth}}(-\eta_t \text{inv}\mathcal{R}_{\mathbf{X}_t}^{\text{orth}}(\mathbf{X}_{t-1}))$,

 exact line search rule $\mu_t = \frac{\|\text{grad } f(\mathbf{Y}_t)\|_F^2}{\|\mathcal{A}(\text{grad } f(\mathbf{Y}_t))\|_2^2}$,

$\mathbf{X}_{t+1} = \mathcal{R}_{\mathbf{Y}_t}^{\text{orth}}(-\mu_t \text{grad } f(\mathbf{Y}_t))$,

end for

Ensure: \mathbf{X}_T .

The extrapolation sequence $\{\mathbf{Y}_t\}$ is strictly restricted to geodesics. Through the inverse orthographic retraction, the following relationship reflects the linear extrapolation on the tangent space (16), i.e.,

$$\text{inv}\mathcal{R}_{\mathbf{X}_t}^{\text{orth}}(\mathbf{Y}_t) = \mathbf{X}_t + \eta_t(\mathbf{X}_t - \text{inv}\mathcal{R}_{\mathbf{X}_t}^{\text{orth}}(\mathbf{X}_{t-1})),$$

A visualization of the extrapolation process is presented in Fig. 1(d). Compared to the non-accelerated Algorithm 4, Algorithm 5 seems to increase the computational cost caused by the extra operators, but the convergence rate is greatly improved. Because the whole process alternates only between the

manifold and tangent space, we can use (26) to achieve a fast transfer of tangent space between $\{\mathbf{X}_t\}$ and $\{\mathbf{Y}_t\}$. Regarding convergence, the iterative matrix of NAG is entirely consistent with NARG, and its derivation is shown in Appendix E.3. Combined with Theorem 2, NAG yields the same local linear convergence rate on Euclidean and manifold. Essentially, this boils down to the same first-order expansion of iterations w.r.t. small perturbations.

Remark 7 Compared with the existing Euclidean acceleration, such as [34, 20], we firstly establish a bidirectional connection between tangent space and manifold by an orthographic retraction from the perspective of Riemannian geometry. Following the framework [36], a new perturbation analysis in Lemma 3 can bridge the gap between Euclidean and manifold.

5 Adaptive Restart Scheme

In practice, optimal estimation of momentum parameters is often challenging. The adaptive restart scheme [28] judges whether the momentum leads in the wrong direction through function or gradient conditions. The convergence rate consistent with the optimal spectral radius is affirmed in applications such as strongly convex quadratic optimization [18], linear elliptic problem [29] and matrix completion [34]. We propose an adaptive restart scheme-based NARG algorithm with low complexity for low-rank matrix estimation; see Algorithm 6.

Algorithm 6 NARG with Adaptive Restart Scheme (NAGR+R)

Require: observation \mathbf{y}_{ob} , rank r , maximum iteration T .

Initialize: $\mathbf{X}_{-1} = \mathbf{X}_0 = \mathcal{A}^*(\mathbf{y}_{\text{ob}})$.

for $t = 0, 1, \dots, T - 1$ **do**

if $\langle \nabla f(\mathbf{Y}_{t-1}), \mathbf{X}_t - \mathbf{X}_{t-1} \rangle > 0$ **then**

$\tau = 1$,

else

$\tau = \tau + 1$,

end if

 set extrapolation $\mathbf{Y}_t = \mathcal{R}_{\mathbf{X}_t}^{\text{orth}}(-\eta_t \text{inv}\mathcal{R}_{\mathbf{X}_t}^{\text{orth}}(\mathbf{X}_{t-1}))$ with $\eta_t = \frac{\tau-1}{\tau+2}$,

 exact line search rule $\mu_t = \frac{\|\text{grad } f(\mathbf{Y}_t)\|_F^2}{\|\mathcal{A}(\text{grad } f(\mathbf{Y}_t))\|_2^2}$,

$\mathbf{X}_{t+1} = \mathcal{R}_{\mathbf{Y}_t}^{\text{orth}}(-\mu_t \text{grad } f(\mathbf{Y}_t))$,

end for

Ensure: \mathbf{X}_T .

Moreover, we establish the equivalence relation of gradient condition between Euclidean and manifold by the tangent space. According to Lemma 3, we find that the sign of the gradient condition is consistent with its expansion in the tangent space, i.e.

$$\begin{aligned} & \text{sign}(\langle \text{grad } f(\mathbf{Y}_{t-1}), \text{inv}\mathcal{R}_{\mathbf{Y}_{t-1}}^{\text{orth}}(\mathbf{X}_t) - \text{inv}\mathcal{R}_{\mathbf{Y}_{t-1}}^{\text{orth}}(\mathbf{X}_{t-1}) \rangle) \\ &= \text{sign}(\langle \nabla f(\mathbf{Y}_{t-1}), \mathbf{X}_t - \mathbf{X}_{t-1} \rangle). \end{aligned} \quad (28)$$

See Appendix E.4 for proof and Fig. 3 for geometric interpretation. Nevertheless, the projection introduces an additional computational cost, so we still use the traditional gradient condition in Algorithm 6. Besides, a practical trick is to perform a restart once condition (8) holds, which can facilitate local approximation and iterative analysis of constraints.

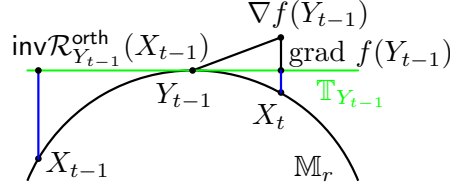


Fig. 3 Illustration of adaptive restart scheme from a manifold point of view.

The following corollary can be established with the optimal spectral radius in Theorem 2.

Corollary 2 (Adaptive Restart Scheme) *Let λ_{\max} and λ_{\min} correspond to the largest and smallest non-zero eigenvalues of $(\mathbf{I} - P_{\mathbf{V}_*}^\perp \otimes P_{\mathbf{U}_*}^\perp)\Theta$, respectively. When condition (8) holds, Algorithm 6 satisfies*

$$\|\mathbf{X}_{t+1} - \mathbf{X}_*\|_F \leq 1 - \sqrt{\frac{4\lambda_{\min}}{\lambda_{\min} + 3\lambda_{\max}}} \|\mathbf{X}_t - \mathbf{X}_*\|_F.$$

6 Numerical Examples

In this section, we provide numerical experiments to confirm our theoretical results, with the Matlab codes available at

<https://github.com/pxxyyz/FastGradient>.

6.1 Convergence for Quadratic Problem

We take the 2-D quadratic problem as an example. Set the symmetric positive definite matrix $\mathbf{Q} = \begin{pmatrix} 10 & 1 \\ 1 & 1 \end{pmatrix}$ and the optimal point $\mathbf{x}_* = (0, 0)^\top$. Let $\mathbf{Q} = \mathbf{V}\mathbf{\Lambda}\mathbf{V}^{-1}$ be the eigen decomposition. Denote the rotation angle of the orthogonal basis as $\alpha = \min_{i=1,2} \arctan(\mathbf{V}_{i,2}/\mathbf{V}_{i,1})$, then $\mathbf{x}_0 = \mathbf{Q}^{-1}(\cos(\alpha + \theta), \sin(\alpha + \theta))^\top$ with $\theta \in [0, 2\pi]$.

We know gradient $\nabla f(\mathbf{x}_0) = (\cos(\alpha + \theta), \sin(\alpha + \theta))^\top$ and stepsize $\tilde{\mu} = \langle \nabla f(\mathbf{x}_0), \mathbf{Q}\nabla f(\mathbf{x}_0) \rangle^{-1}$. The relationship (15) is verified in Fig. 4. In particular, when $\theta = (1 \pm 2k)\pi/4$, the convergence rate reaches the upper bound and is the same as the optimal constant stepsize, which verifies $\hat{\mu} = \tilde{\mu} = 2/(\lambda_{\max} + \lambda_{\min})$

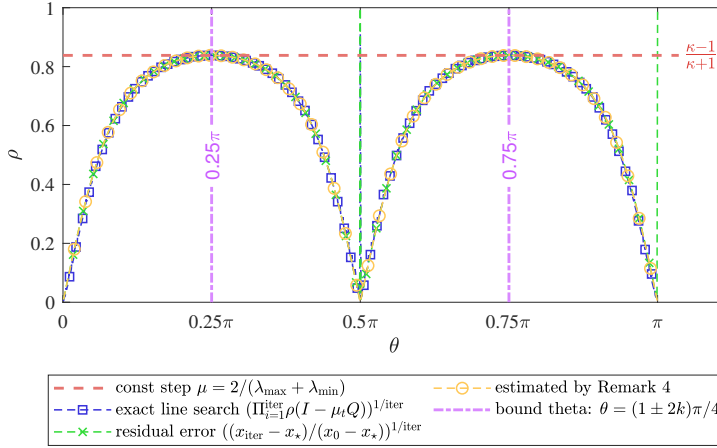


Fig. 4 Relationship between Convergence Rate and θ under Exact Line Search.

in Remark 5. When $\theta = k/2\pi$, \mathbf{x}_0 is located in the direction of the eigenvector, and the gradient points to \mathbf{x}_* . The stepsize equals the corresponding eigenvalue, so it takes one step to reach \mathbf{x}_* , consistent with [13].

6.2 MC and MS

Under different ranks and numbers of observations, we test the performance of algorithms and verify the validity of converged estimates. Comparison methods include IHT, NIHT [31], Grad, RGrad, NAG, NARG, and NARG+R, where NIHT uses the first stepsize in Remark 6, and the last uses the restart scheme. The accelerated algorithms, including NAG and NARG, use the Lazy strategy with $d = 2$. Since there are two retractions, we use RGrad-Proj and RGrad-Orth to distinguish them. The simulations of MC and MS are shown in Fig. 5 and Fig. 6, respectively. Here, the dashed line and the dash-dotted line compare the actual and estimated errors of the algorithm. The brackets in the legend record the algorithm running time. And ρ is an estimate of the convergence rate, which reflects the slope of the linear decline. It is worth mentioning that we use the optimal spectral radius of Theorem 2 as the optimal convergence rate of the accelerated algorithm.

From the comparison results, the estimation of the convergence rate of all algorithms is convincing. The spectral radii of the first five methods are close, but the manifold-based methods dominate in terms of running time. This also holds for comparing accelerated algorithms, namely NAG and NARG. On the one hand, efficient retraction reduces the overall computational complexity and thus significantly reduces the running time under the premise of the same convergence rate. On the other hand, the convergence rate is related to the iterative method but not the geometry, which also reflects Lemma 3. Furthermore, for the accelerated methods, the high momentum under-damping causes

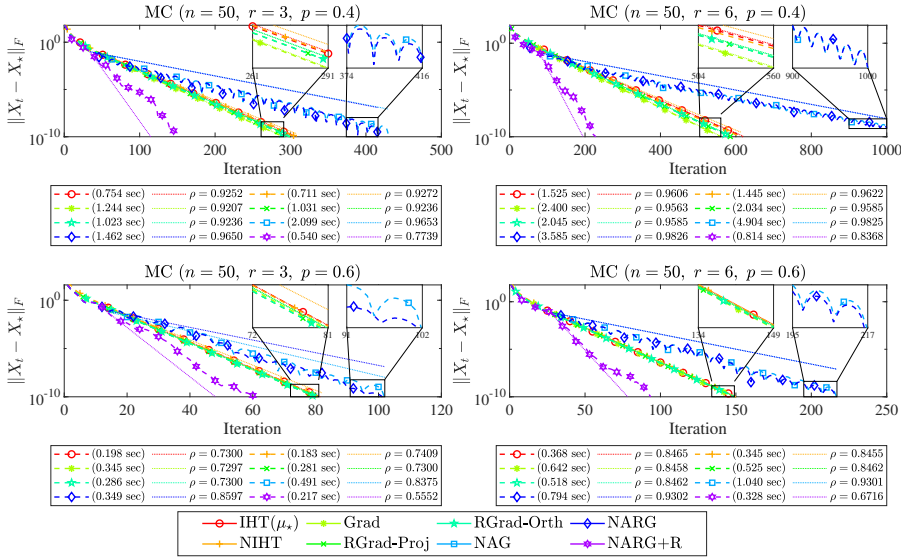


Fig. 5 (Log-scale) plot of error in MC.

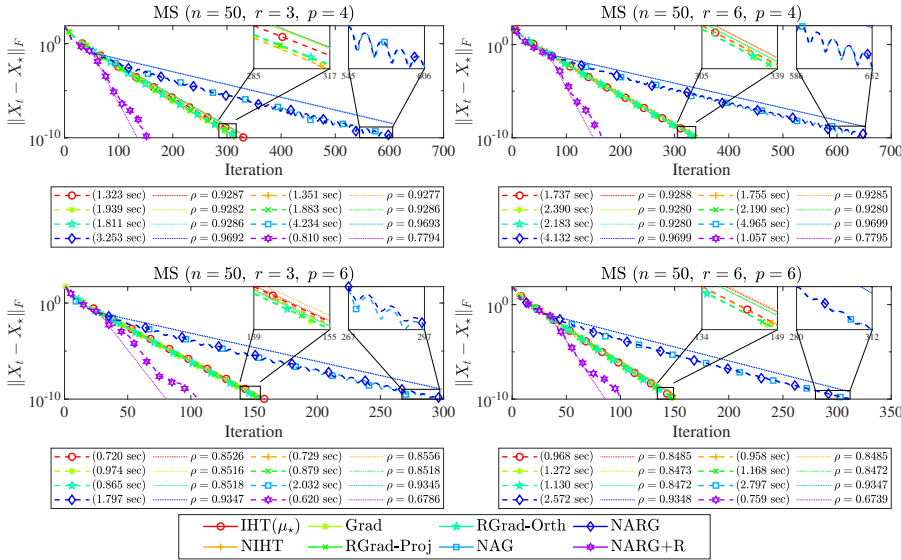


Fig. 6 (Log-scale) plot of error in MS.

the rippling behavior as the iterations increase. The adaptive restart scheme can avoid ripples and matches the optimal convergence rate, confirming Corollary 2. Overall, the latest algorithm prevails on both sides.

6.3 Oscillation caused by momentum

To further illustrate the relationship between momentum and acceleration, we show the oscillatory effect under different parameters divided into two cases. When the optimal parameter is known, as suggested in [28], we set $\eta_t \equiv \frac{1-\sqrt{q}}{1+\sqrt{q}}$ and $q^* = \kappa^{-1}$. We observe the damping effect at different q in Fig. 7. When $q < q^*$, momentum higher than the optimal parameter will cause oscillations to slow the convergence rate. Conversely, when $q > q^*$, as q increases, the gradually decreasing spectral radius makes the convergence slower. Until $q = 1$, i.e., $\eta_t \equiv 0$, the momentum does not work, and the accelerated algorithm degenerates to the original algorithm. The result of $q = q^*$ is optimal and consistent with the trend of NARG+R.

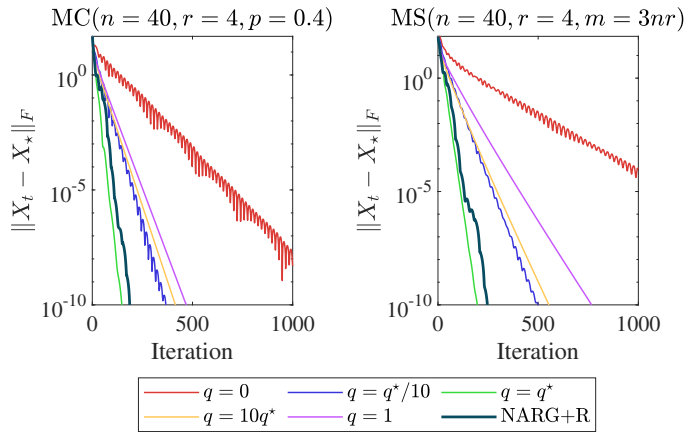


Fig. 7 Rippling behavior under different momentum parameter settings.

When the optimal parameter is unknown, we set $\eta_t = \frac{t-1}{t+d}$ by referring to the discussion of heuristic momentum [24, 25]. We compared different $d = 2, 5, 10, 20$ in Fig. 8. As d increases, the convergence is improved. According to the average speed in (19), when d increases, the slower η_t grows, and the longer it stays around the optimal parameter, the lower the convergence rate ρ is.

6.4 Estimation of Spectral Radius

Below we verify the spectral radius estimation of the iterative matrix in conclusion, which is the key to the convergence analysis for all algorithms. We plot the spectral radius of MC and MS under different step sizes and different numbers of observations in Fig. 9. The coincidence of actual spectral radius (solid lines) and its estimation (dashed lines) verifies that the relationship (9) holds. There are some differences in stepsize in (11) between MC and MS.

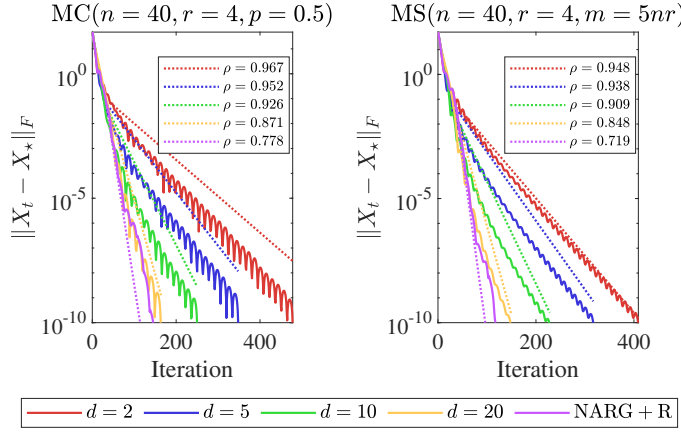


Fig. 8 Convergence comparison of lazy strategy with different d .

As the number of observations increases, the optimal stepsize μ_{\dagger} and upper bound μ_{\ddagger} for MS increase, while the results for MS are reversed. But, there are obvious upper bounds $\mu_{\ddagger} < 1$ for MS and $\mu_{\ddagger} < 2$ for MC.

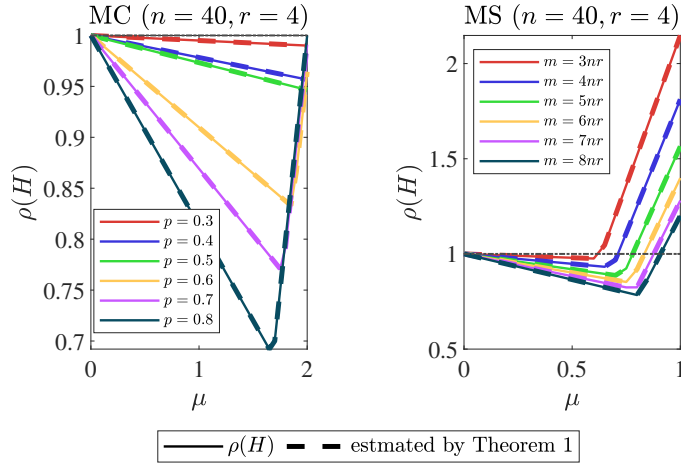


Fig. 9 Spectral radius estimation of Algorithm 1.

Fig. 10 shows that there is a complex 3-D relationship between the spectral radius of the iterative matrix in (17) and parameter pair (μ, η) . For a more intuitive presentation, we give its contour in Fig. 11, which verifies our solution to the equation (31). It can be seen that there is an apparent intersection (green dashed line) between the surfaces Π_1 and Π_2 . Moreover, the global minimum is on the junction of $\Delta \geq 0$ (pink area) and the green dash. We accurately label the estimates of the optimal parameters with a circle according to Theorem 2.

The yellow line corresponding to $\mu > \mu_{\dagger}$ means that introducing momentum does not improve algorithm convergence.

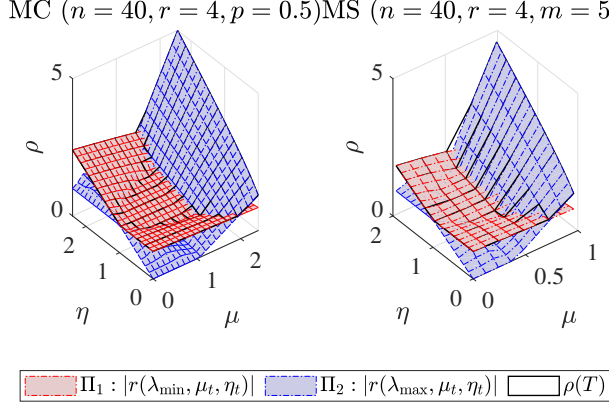


Fig. 10 3D surface relationship between spectral radius and (μ, η) .

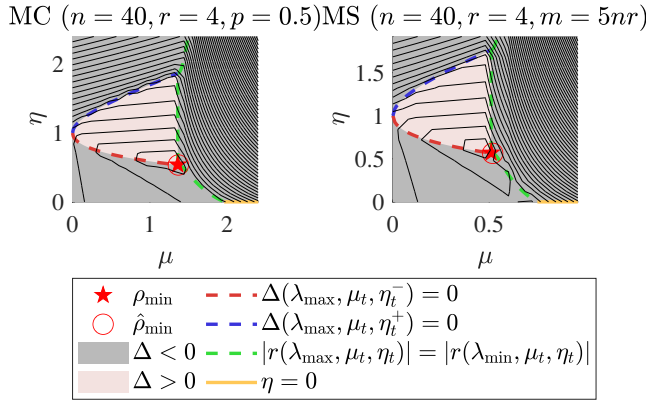


Fig. 11 2D Top view of spectral radius w.r.t. (μ, η) .

In addition, we also plot the relationship between the spectral radius individually w.r.t. μ or η , respectively. Fig. 12 verifies the staged estimates of spectral radius in Appendix D. The blue line of Fig. 12 is equivalent to the yellow line of Fig. 11 and the rising part of Fig. 9. The spectral radius of μ_{\dagger} and μ_b correspond to the optimal convergence rates of the accelerated and original algorithms.

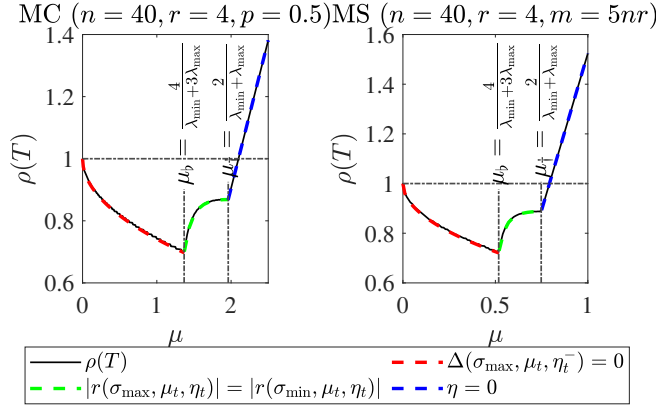


Fig. 12 Spectral radius estimation of Algorithm 3.

6.5 Runtime comparison for larger simulations

Under the setting of different parameters (n, r, p) , the proposed NARG+R algorithm is compared with the state-of-the-art algorithms, including RGrad and ScaledGD [32]. Table 2 presents the average number of iterations and runtime over 20 random simulations with the stopping condition $\|\mathbf{X}_t - \mathbf{X}_*\|_F \leq 10^{-8}$. By contrast, the matrix size does not affect the number of iterations of the three algorithms. When p is larger and r is smaller, algorithms for MC usually converge faster. Similarly, the larger p is, the faster the algorithm for MS. The impact of the parameter (p, r) will be discussed later. Overall, the proposed NARG+R has a significant advantage in the number of iterations, which shows that it is competitive in large-scale matrix applications.

6.6 Spectral initialization versus Random initialization

Taking RGrad as an example, we analyze the impact of initialization, and its settings are shown in Table 3. Random initialization adds Gaussian noise with different variances based on spectral initialization [9]. The comparisons are shown in Fig. 13. The results show that random initialization has a more significant impact on MC. As σ increases, random initialization moves the unobserved further away from the optimal solution, which makes the algorithm more challenging to satisfy (8). In contrast, spectral initialization speeds up the process, dramatically improving local search efficiency. On the other hand, MS is less affected by initialization, and linear convergence requires only a few iterations. Once condition (8) holds, the local convergence rate is independent of initialization and is related to the spectral radius.

Table 2 Average number of iterations and average runtime (seconds) over 20 random simulations.

Algorithm	Iter	Time	Iter	Time	Iter	Time	Iter	Time
MC, $n = 2500$, sample size n^2p								
	$r = 0.05n, p = 0.4$		$r = 0.05n, p = 0.6$		$r = 0.1n, p = 0.4$		$r = 0.1n, p = 0.6$	
RGrad	72.7	13.407	38.9	7.756	198	54.03	69	19.848
Scaled GD	145	25.508	92	17.27	360.7	93.906	157	42.814
NARG+R	56	11.11	33.25	7.092	123.5	35.56	55	16.62
MC, $n = 5000$, sample size n^2p								
	$r = 0.05n, p = 0.4$		$r = 0.05n, p = 0.6$		$r = 0.1n, p = 0.4$		$r = 0.1n, p = 0.6$	
RGrad	74	69.898	40	40.418	203	323.2	71	117.31
Scaled GD	149	136.28	95	91.996	371.45	560.61	162	253.78
NARG+R	59	59.225	35	37.25	129	212.69	55	93.698
MS, $n = 100$, sample size pnr								
	$r = 0.05n, p = 4$		$r = 0.05n, p = 6$		$r = 0.1n, p = 4$		$r = 0.1n, p = 6$	
RGrad	319.1	6.7832	135.8	4.4625	303.55	12.821	131.75	8.237
Scaled GD	425.7	6.3149	207.4	4.7171	404.7	11.8	200.5	8.7509
NARG+R	144.8	3.0753	81.7	2.6768	136.55	5.7343	89.7	5.595
MS, $n = 200$, sample size pnr								
	$r = 0.05n, p = 4$		$r = 0.05n, p = 6$		$r = 0.1n, p = 4$		$r = 0.1n, p = 6$	
RGrad	337.6	71.826	142.95	45.913	320.2	135.86	138.8	88.308
Scaled GD	450.45	63.297	217.35	45.782	425.8	118.98	210.4	88.039
NARG+R	154.75	32.835	80.6	25.718	171.95	72.79	81	51.26

Table 3 Initialization settings.

	Spectral initialization	Random initialization
MC	$\mathbf{X}_0 = \mathcal{P}_r(\frac{1}{p}\mathcal{P}_\Omega(\mathbf{X}_{\text{ob}}))$	$\mathbf{X}_0 = \mathcal{P}_r(\frac{1}{p}\mathcal{P}_\Omega(\mathbf{X}_{\text{ob}}) + \mathcal{P}_{\Omega^c}(\mathbf{Y}_{\text{rand}}))$ $[\mathbf{Y}_{\text{rand}}]_{i,j} \sim \mathcal{N}(0, \sigma^2)$
MS	$\mathbf{X}_0 = \mathcal{P}_r(\mathcal{A}^*(\mathbf{y}_{\text{ob}}))$	$\mathbf{X}_0 = \mathcal{P}_r(\mathcal{A}^*(\mathbf{y}_{\text{ob}} + \mathbf{y}_{\text{rand}}))$ $[\mathbf{y}_{\text{rand}}]_i \sim \mathcal{N}(0, \sigma^2)$

6.7 Numerical phase transition

Finally, we evaluate and compare the recovery rate of NARG+R with ScaledGD and RGrad. If $\|\hat{\mathbf{X}} - \mathbf{X}_\star\|_F \leq 10^{-3}$, we judge it as a successful recovery, where $\hat{\mathbf{X}}$ is the output of the algorithm. The empirical success rate was calculated by repeating 20 trials with different ranks and sample sizes. For sample size, we use sampling rate $p = |\Omega|/n^2$ for MC and $m = pnr$ for MS. The empirical phase transitions are presented in Fig. 14, where white indicates successful recovery and black indicates failure for NARG+R. Our algorithm produces a more extensive white area on both tasks than the others. The theoretical lower bound for estimating sample size using the iterative matrix is still an open problem, and we leave it as future work.

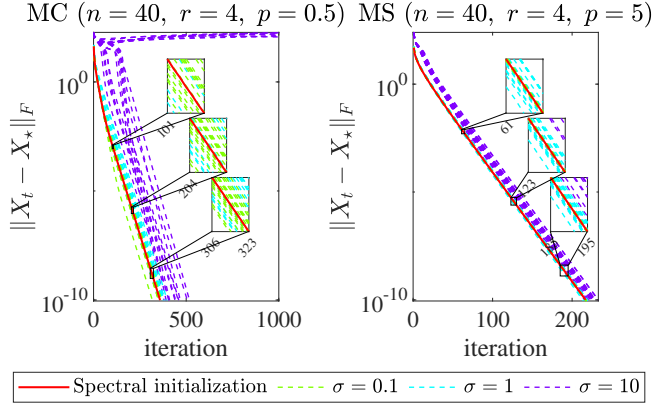


Fig. 13 Comparison of Spectral initialization and Random initialization with different σ .

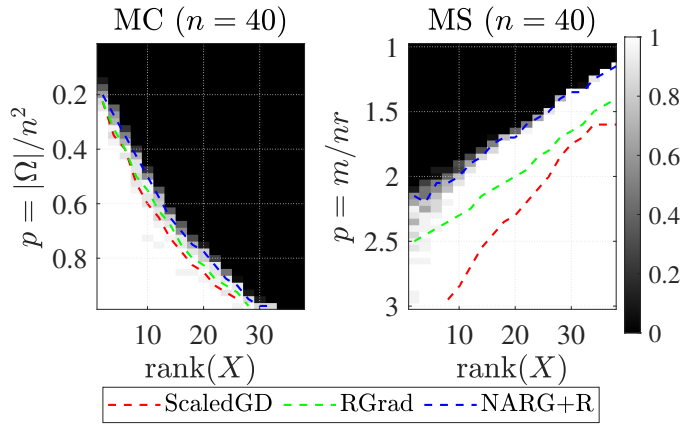


Fig. 14 Phase transition of NARG+R for MC and MS over 20 random simulations. The dotted line indicates that the success rate of all methods reaches 50%, which serves as a reference for comparison.

7 Conclusion

We have proposed a novel efficient Nesterov’s Accelerated Riemannian Gradient for the low-rank matrix estimation problem. To our knowledge, this is the first work to connect manifold and tangent space through orthographic retraction and its inverse. As the name suggests, it inherits the low computational complexity of the Riemannian Gradient and the fast linear convergence rate of Nesterov’s Accelerated Gradient. The spectral radius estimates the local convergence rate. The algorithm matches the theoretical optimal rate based on the adaptive restart scheme. Numerical simulations of both MS and MC illustrate that our algorithm is superior in computational complexity. It would be interesting to study theoretical optimal sample complexity by the spectral

radius of the iterative matrix. Another further direction is the generalization to tensors, such as Tucker decomposition and Tensor-Train decomposition.

A Auxiliary lemmas

A.1 Relationship of matrix eigenvalues

Lemma 4 *Let Θ be a symmetric positive semi-definite matrix, and $P \in \mathbb{R}^{n \times n}$ be an orthogonal projection matrix. Denote $P^\perp = I - P$, then there exists an eigenvalue $\lambda \neq 0$ of $(I - \mu\Theta)P^\perp$, such that*

$$\lambda_i(\mu\Theta P^\perp + P) = \lambda_i(\mu\Theta P^\perp) = 1 - \lambda.$$

Proof Assume $\text{rank}(P) = r$. According to idempotent, we get the eigenvalues of P and P^\perp of the form.

$$\lambda(P) = \{\underbrace{1, \dots, 1}_r, \underbrace{0, \dots, 0}_{n-r}\}, \lambda(P^\perp) = \{\underbrace{1, \dots, 1}_{n-r}, \underbrace{0, \dots, 0}_r\}.$$

Here, we use \mathbf{u}_i and \mathbf{v}_j represent the eigenvectors of P corresponding to eigenvalues 1 and 0, respectively. From the orthogonal relation between P and P^\perp , $P\mathbf{u}_i = \mathbf{u}_i$, $P\mathbf{v}_j = \mathbf{0}$, $P^\perp\mathbf{u}_i = \mathbf{0}$, $P^\perp\mathbf{v}_j = \mathbf{v}_j$. Further, we have

$$(\mu\Theta P^\perp + P)\mathbf{u}_i = \mathbf{u}_i, (\mu\Theta P^\perp)\mathbf{u}_i = \mathbf{0}, (\mu\Theta P^\perp + P)\mathbf{v}_j = (\mu\Theta P^\perp)\mathbf{v}_j = \mu\Theta\mathbf{v}_j. \quad (29)$$

It can be known that \mathbf{u}_i corresponds to the eigenvector of $\mu\Theta P^\perp + P$ with the eigenvalue of 1 and the eigenvector of $\mu\Theta P^\perp$ with the eigenvalue of 0, respectively. Besides, if \mathbf{v}_j happens to be an eigenvector of $\mu\Theta$, then \mathbf{v}_j is also an eigenvector of $\mu\Theta P^\perp + P$ and $\mu\Theta P^\perp$. This conjecture implies the relevance of the above three matrix eigendecompositions. To this end, assume that there exists a non-zero vector \mathbf{x} such that

$$(I - \mu\Theta)P^\perp\mathbf{x} = \lambda\mathbf{x},$$

then

$$(\mu\Theta P^\perp + P)\mathbf{x} = (1 - \lambda)\mathbf{x}.$$

For $\lambda \neq 0$, we will discuss $P\mathbf{x} = (1 - \lambda)\mathbf{x} - \mu\Theta P^\perp\mathbf{x}$ case by case:

Case 1: when $P\mathbf{x} = \mathbf{0}$, i.e., \mathbf{x} is a linear combination of \mathbf{v}_i . Obviously, $\mu\Theta P^\perp\mathbf{x} = (1 - \lambda)\mathbf{x}$ holds. We obtain $1 - \lambda$ is the eigenvalue of matrix $\mu\Theta P^\perp$.

Case 2: when $P\mathbf{x} \neq \mathbf{0}$, we know that \mathbf{x} can always be represented as a linear combination of orthonormal bases, as follows

$$\mathbf{x} = \sum_{i=1}^r \alpha_i \mathbf{u}_i + \sum_{j=1}^{n-r} \beta_j \mathbf{v}_j,$$

and $P\mathbf{x} \neq \mathbf{0}$ means that there exists $\alpha_i \neq 0$, otherwise $P\mathbf{x} = \sum_{j=1}^{n-r} \beta_j P\mathbf{v}_j = \mathbf{0}$ if $\forall i, \alpha_i = 0$. And we expand the formula to get

$$(I - \mu\Theta) \sum_{j=1}^{n-r} \beta_j \mathbf{v}_j = (I - \mu\Theta)P^\perp\mathbf{x} = \lambda\mathbf{x} = \lambda \left(\sum_{i=1}^r \alpha_i \mathbf{u}_i + \sum_{j=1}^{n-r} \beta_j \mathbf{v}_j \right),$$

where the left-hand side is a linear representation of the basis vector $\{\mathbf{v}_j\}$, while the right-hand side is a linear combination of mutually orthogonal basis vectors $\{\mathbf{u}_i\}$ and $\{\mathbf{v}_j\}$. So when $\lambda \neq 0$, $\forall i, \alpha_i = 0$ holds. This contradicts $P\mathbf{x} \neq \mathbf{0}$. \square

A.2 Perturbation Analysis of Subspaces

Lemma 5 (Wedin's $\sin \Theta$ Theorem [8]) Let $\mathbf{X}_t = \mathbf{U}_t \boldsymbol{\Sigma}_t \mathbf{V}_t^\top$ and $\mathbf{X}_\star = \mathbf{U}_\star \boldsymbol{\Sigma}_\star \mathbf{V}_\star^\top$ be the SVD of $\mathbf{X}_t, \mathbf{X}_\star \in \mathbb{M}_r$, respectively. If $\|\mathbf{X}_t - \mathbf{X}_\star\| < \sigma_r(\mathbf{X}_\star)$, there is an upper bound for the perturbation of the singular subspace as follows

$$\max\{\|P_{\mathbf{U}_t}^\perp - P_{\mathbf{U}_\star}^\perp\|, \|P_{\mathbf{V}_t}^\perp - P_{\mathbf{V}_\star}^\perp\|\} \leq \frac{2\|\mathbf{X}_t - \mathbf{X}_\star\|}{\sigma_r(\mathbf{X}_\star)}.$$

Lemma 6 (Perturbation of subspace projection [40]) Let $\mathbf{X}_t = \mathbf{U}_t \boldsymbol{\Sigma}_t \mathbf{V}_t^\top$ and $\mathbf{X}_\star = \mathbf{U}_\star \boldsymbol{\Sigma}_\star \mathbf{V}_\star^\top$ be the SVD of $\mathbf{X}_t, \mathbf{X}_\star \in \mathbb{M}_r$, respectively. If $\|\mathbf{X}_t - \mathbf{X}_\star\| < \sigma_r(\mathbf{X}_\star)$, then the following inequality is satisfied

$$\|P_{\mathbf{U}_\star}^\perp \mathbf{X}_t P_{\mathbf{V}_\star}^\perp\|_F \leq \frac{\|\mathbf{X}_t - \mathbf{X}_\star\|_F^2}{\sigma_r(\mathbf{X}_\star)}.$$

B Proof of Theorem 1

Proof Let the residual matrix $\mathbf{E}_t = \mathbf{X}_t - \mathbf{X}_\star$. According to the iteration, we have

$$\begin{aligned} \mathbf{E}_{t+1} &= \mathbf{X}_{t+1} - \mathbf{X}_\star \\ &= \mathcal{P}_r(\mathbf{X}_t - \mu_t \nabla f(\mathbf{X}_t)) - \mathbf{X}_\star \\ &= \mathcal{P}_r(\mathbf{X}_\star + \mathbf{X}_t - \mathbf{X}_\star - \mu_t \nabla f(\mathbf{X}_t)) - \mathbf{X}_\star \\ &= \mathcal{P}_r(\mathbf{X}_\star + \mathbf{E}_t - \mu_t \nabla f(\mathbf{X}_t)) - \mathbf{X}_\star \\ &\stackrel{(a)}{=} (\mathbf{E}_t - \mu_t \nabla f(\mathbf{X}_t)) - P_{\mathbf{U}_\star}^\perp (\mathbf{E}_t - \mu_t \nabla f(\mathbf{X}_t)) P_{\mathbf{V}_\star}^\perp + \mathcal{O}(\|\mathbf{E}_t\|_F^2), \end{aligned} \quad (30)$$

where (a) is the first-order expansion (7) of the truncated SVD. Since $\|\mathcal{I} - \mu_t \mathbf{A}^* \mathbf{A}\| \leq 1$, we have $\|\mathbf{E}_t - \mu_t \nabla f(\mathbf{X}_t)\|_F = \|(\mathcal{I} - \mu_t \mathbf{A}^* \mathbf{A})(\mathbf{E}_t)\|_F \leq \|\mathbf{E}_t\|_F \leq \sigma_r(\mathbf{X}_\star)/2$, which verifies the condition of Lemma 1 holds. After vectorizing $\mathbf{e}_{t+1} = \text{vec}(\mathbf{E}_{t+1})$, we get

$$\begin{aligned} \mathbf{e}_{t+1} &= \text{vec}((\mathbf{E}_t - \mu_t \nabla f(\mathbf{X}_t)) - P_{\mathbf{U}_\star}^\perp (\mathbf{E}_t - \mu_t \nabla f(\mathbf{X}_t)) P_{\mathbf{V}_\star}^\perp) + \mathcal{O}(\|\mathbf{E}_t\|_F^2) \\ &\stackrel{(a)}{=} (\mathbf{I} - P_{\mathbf{V}_\star}^\perp \otimes P_{\mathbf{U}_\star}^\perp) \text{vec}(\mathbf{E}_t - \mu_t \nabla f(\mathbf{X}_t)) + \mathcal{O}(\|\mathbf{E}_t\|_F^2) \\ &\stackrel{(b)}{=} \underbrace{(\mathbf{I} - P_{\mathbf{V}_\star}^\perp \otimes P_{\mathbf{U}_\star}^\perp)}_{\mathbf{H}(\mu_t)} (\mathbf{I} - \mu_t \boldsymbol{\Theta}) \mathbf{e}_t + \mathcal{O}(\|\mathbf{e}_t\|_2^2), \end{aligned}$$

where (a) uses vectorization of Kronecker product, i.e., $\text{vec}(\mathbf{ABC}) = (\mathbf{C}^\top \otimes \mathbf{A})\text{vec}(\mathbf{B})$. (b) is based on (3) and $\|\mathbf{E}_t\|_F = \|\mathbf{e}_t\|_2$. The convergence rate with the constant stepsize $\mu_t \equiv \mu$ is determined by the spectral radius of the matrix $\mathbf{H} = \mathbf{H}(\mu)$.

$$\rho(\mathbf{H}) = \max_\lambda |\lambda_i(\mathbf{H})| = \max(|\lambda_{\max}(\mathbf{H})|, |\lambda_{\min}(\mathbf{H})|).$$

Thus, the maximum and minimum eigenvalues of \mathbf{H} should be compared. Taking MS as an example, we compute the largest eigenvalue.

$$\begin{aligned} \lambda_{\max}(\mathbf{H}_{\text{MS}}) &= 1 - \lambda_{\min}(\mu \boldsymbol{\Theta} + P_{\mathbf{V}_\star}^\perp \otimes P_{\mathbf{U}_\star}^\perp - \mu(P_{\mathbf{V}_\star}^\perp \otimes P_{\mathbf{U}_\star}^\perp) \boldsymbol{\Theta}) \\ &\stackrel{(a)}{=} 1 - \lambda_{\min}(\mu \boldsymbol{\Theta} - \mu(P_{\mathbf{V}_\star}^\perp \otimes P_{\mathbf{U}_\star}^\perp) \boldsymbol{\Theta}) \\ &= 1 - \mu \lambda_{\min}((\mathbf{I} - P_{\mathbf{V}_\star}^\perp \otimes P_{\mathbf{U}_\star}^\perp) \boldsymbol{\Theta}), \end{aligned}$$

where (a) is based on Lemma 4. Similarly, the minimum eigenvalue results are as follows:

$$\lambda_{\min}(\mathbf{H}_{\text{MS}}) = 1 - \mu \lambda_{\max}((\mathbf{I} - P_{\mathbf{V}_\star}^\perp \otimes P_{\mathbf{U}_\star}^\perp) \boldsymbol{\Theta}).$$

Obviously, the optimal spectral radius occurs when $\lambda_{\max}(\mathbf{H}_{\text{MS}}) = -\lambda_{\min}(\mathbf{H}_{\text{MS}})$, i.e., $1 - \mu\lambda_{\min} = \mu\lambda_{\max} - 1$. The corresponding stepsize is $\mu_{\dagger} = \frac{2}{\lambda_{\min} + \lambda_{\max}}$. Due to $\mathbf{I} - P_{\mathbf{V}_*}^{\perp} \otimes P_{\mathbf{U}_*}^{\perp}$ is orthogonal projector, we have $\|\mathbf{I} - P_{\mathbf{V}_*}^{\perp} \otimes P_{\mathbf{U}_*}^{\perp}\| = 1$. It is easy to check

$$\rho(\mathbf{H}) \leq \|\mathbf{I} - P_{\mathbf{V}_*}^{\perp} \otimes P_{\mathbf{U}_*}^{\perp}\| \|\mathbf{I} - \mu_t \boldsymbol{\Theta}\| \leq \|\mathbf{I} - \mu_t \boldsymbol{\Theta}\| \leq 1,$$

so we can get (9). Especially for MC, as shown in (6), we get a simplified result similar to [34].

$$\begin{aligned} \lambda_{\max}(\mathbf{H}_{\text{MC}}) &\stackrel{(a)}{=} 1 - \mu\lambda_{\min}(\mathbf{S}_{\Omega}^{\top}(\mathbf{I} - P_{\mathbf{V}}^{\perp} \otimes P_{\mathbf{U}}^{\perp})\mathbf{S}_{\Omega}) \stackrel{(b)}{=} 1 - \mu\lambda_{\min}(\mathbf{I} - \mathbf{S}_{\Omega}^{\top}(P_{\mathbf{V}_*}^{\perp} \otimes P_{\mathbf{U}_*}^{\perp})\mathbf{S}_{\Omega}) \\ &= 1 - \mu(1 - \lambda_{\max}(\mathbf{S}_{\Omega}^{\top}(P_{\mathbf{V}_*}^{\perp} \otimes P_{\mathbf{U}_*}^{\perp})\mathbf{S}_{\Omega})) \stackrel{(c)}{=} 1 - \mu(1 - \lambda_{\max}(\mathbf{S}_{\Omega}\mathbf{S}_{\Omega}^{\top}(P_{\mathbf{V}_*}^{\perp} \otimes P_{\mathbf{U}_*}^{\perp}))) \\ &\stackrel{(d)}{=} 1 - \mu(\lambda_{\min}(P_{\mathbf{V}_*}^{\perp} \otimes P_{\mathbf{U}_*}^{\perp} - \mathbf{S}_{\Omega}\mathbf{S}_{\Omega}^{\top}(P_{\mathbf{V}_*}^{\perp} \otimes P_{\mathbf{U}_*}^{\perp}))) \stackrel{(e)}{=} 1 - \mu(\lambda_{\min}(\mathbf{S}_{\Omega}\mathbf{S}_{\Omega}^{\top}(P_{\mathbf{V}_*}^{\perp} \otimes P_{\mathbf{U}_*}^{\perp}))) \\ &\stackrel{(f)}{=} 1 - \mu(\lambda_{\min}(\mathbf{S}_{\Omega}^{\top}(P_{\mathbf{V}_*}^{\perp} \otimes P_{\mathbf{U}_*}^{\perp})\mathbf{S}_{\Omega})) = 1 - \mu(\sigma_{\min}^2(\mathbf{S}_{\Omega}^{\top}(\mathbf{V}_* \perp \otimes \mathbf{U}_* \perp))), \end{aligned}$$

where (a), (c) and (f) are based on the fact that AB and BA have the same eigenvalues, (b) and (e) correspond to the properties of the sampling matrix in (6), (d) uses Lemma 4. Similarly, the minimum eigenvalue results are as follows

$$\lambda_{\min}(\mathbf{H}_{\text{MC}}) = 1 - \mu(\sigma_{\max}^2(\mathbf{S}_{\Omega}^{\top}(\mathbf{V}_* \perp \otimes \mathbf{U}_* \perp))).$$

We can estimate the convergence rate of Algorithm 1. \square

C Proof of Proposition 1

Proof Vectorizing (12) yields $\nabla_{\mathcal{R}} f(\mathbf{x}_t) = \mathbf{P}\nabla f(\mathbf{x}_t)$, where $\mathbf{P} = (\mathbf{I} - P_{\mathbf{U}}^{\perp} \otimes P_{\mathbf{V}}^{\perp})$ is the orthogonal projection matrix. Bring (13) into the loss function to get

$$\begin{aligned} f(\mathbf{x}_{t+1}) &= \frac{1}{2}(\mathbf{x}_{t+1} - \mathbf{x}_*)^{\top} \boldsymbol{\Theta}(\mathbf{x}_{t+1} - \mathbf{x}_*) \\ &= \frac{1}{2}(\mathbf{x}_t - \mu_t \nabla_{\mathcal{R}} f(\mathbf{x}_t) - \mathbf{x}_*)^{\top} \boldsymbol{\Theta}(\mathbf{x}_t - \mu_t \nabla_{\mathcal{R}} f(\mathbf{x}_t) - \mathbf{x}_*) + \mathcal{O}(\|\mathbf{x}_t - \mathbf{x}_*\|_2^2) \\ &= f(\mathbf{x}_t) - \mu_t \nabla_{\mathcal{R}} f(\mathbf{x}_t)^{\top} \nabla f(\mathbf{x}_t) + \frac{\mu_t^2}{2} \nabla_{\mathcal{R}} f(\mathbf{x}_t)^{\top} \boldsymbol{\Theta} \nabla_{\mathcal{R}} f(\mathbf{x}_t) + \mathcal{O}(\|\mathbf{x}_t - \mathbf{x}_*\|_2^2) \\ &= f(\mathbf{x}_t) - \frac{(\nabla_{\mathcal{R}} f(\mathbf{x}_t)^{\top} \nabla f(\mathbf{x}_t))^2}{2 \nabla_{\mathcal{R}} f(\mathbf{x}_t)^{\top} \boldsymbol{\Theta} \nabla_{\mathcal{R}} f(\mathbf{x}_t)} + \mathcal{O}(\|\mathbf{x}_t - \mathbf{x}_*\|_2^2) \\ &\stackrel{(a)}{=} \left(1 - \frac{(\nabla_{\mathcal{R}} f(\mathbf{x}_t)^{\top} \nabla f(\mathbf{x}_t))^2}{(\nabla f(\mathbf{x}_t)^{\top} (\mathbf{P}\boldsymbol{\Theta}\mathbf{P}) \nabla f(\mathbf{x}_t)) (\nabla_{\mathcal{R}} f(\mathbf{x}_t)^{\top} (\mathbf{P}\boldsymbol{\Theta}\mathbf{P}) + \nabla_{\mathcal{R}} f(\mathbf{x}_t))} \right) f(\mathbf{x}_t) + \mathcal{O}(\|\mathbf{x}_t - \mathbf{x}_*\|_2^2) \\ &\stackrel{(b)}{\leq} \left(1 - \frac{4}{\frac{\lambda_{\max}(\mathbf{P}\boldsymbol{\Theta}\mathbf{P})}{\lambda_{\min}(\mathbf{P}\boldsymbol{\Theta}\mathbf{P})} + 2 + \frac{\lambda_{\min}(\mathbf{P}\boldsymbol{\Theta}\mathbf{P})}{\lambda_{\max}(\mathbf{P}\boldsymbol{\Theta}\mathbf{P})}} \right) f(\mathbf{x}_t) + \mathcal{O}(\|\mathbf{x}_t - \mathbf{x}_*\|_2^2) \\ &\stackrel{(c)}{\leq} \left(\frac{\kappa - 1}{\kappa + 1} \right)^2 f(\mathbf{x}_t) + \mathcal{O}(\|\mathbf{x}_t - \mathbf{x}_*\|_2^2), \end{aligned}$$

where (a) is because of $f(\mathbf{x}) = \frac{1}{2}(\mathbf{x} - \mathbf{x}_*)^{\top} \boldsymbol{\Theta}(\mathbf{x} - \mathbf{x}_*) = \frac{1}{2} \nabla_{\mathcal{R}} f(\mathbf{x})^{\top} (\mathbf{P}\boldsymbol{\Theta}\mathbf{P}) + \nabla_{\mathcal{R}} f(\mathbf{x})$. Furthermore, since $\frac{|\nabla_{\mathcal{R}} f(\mathbf{x}_t)^{\top} \nabla f(\mathbf{x}_t)|}{\|\nabla_{\mathcal{R}} f(\mathbf{x}_t)^{\top}\|_2 \|\nabla f(\mathbf{x}_t)\|_2} \geq 0$, we apply the generalized Kantorovich type inequality [14] in Lemma 7 to get (b). To prove (c), we only need to show

$$\begin{aligned} \frac{\lambda_{\max}(\mathbf{P}\boldsymbol{\Theta}\mathbf{P})}{\lambda_{\min}(\mathbf{P}\boldsymbol{\Theta}\mathbf{P})} &= \|\mathbf{P}\boldsymbol{\Theta}\mathbf{P}\| \|(\mathbf{P}\boldsymbol{\Theta})^+ \mathbf{P}^+\| \leq \|\mathbf{P}\boldsymbol{\Theta}\| \|\mathbf{P}\| \|\mathbf{P}^+\| \|(\mathbf{P}\boldsymbol{\Theta})^+\| \\ &= \|\mathbf{P}\boldsymbol{\Theta}\| \|(\mathbf{P}\boldsymbol{\Theta})^+\| = \frac{\lambda_{\max}(\mathbf{P}\boldsymbol{\Theta})}{\lambda_{\min}(\mathbf{P}\boldsymbol{\Theta})} := \kappa, \end{aligned}$$

here, $\lambda_{\min}(\cdot)$ means the smallest non-zero eigenvalue. \square

Lemma 7 (Kantorovich inequality [14]) Let \mathbf{A} be a symmetric (semi-) positive definite matrix, and λ_{\max} and λ_{\min} correspond to the largest and smallest non-zero eigenvalues, respectively. If $\mathbf{x}, \mathbf{y} \in \mathbb{R}^n$ satisfies $\frac{|\mathbf{x}^\top \mathbf{y}|}{\|\mathbf{x}\|_2 \|\mathbf{y}\|_2} \geq \cos \theta$ with $0 \leq \theta \leq \frac{\pi}{2}$, then

$$\frac{(\mathbf{x}^\top \mathbf{y})^2}{(\mathbf{x}^\top \mathbf{A} \mathbf{x})(\mathbf{y}^\top \mathbf{A}^+ \mathbf{y})} \geq \frac{4}{\kappa + 2 + \kappa^{-1}},$$

where $\kappa = \frac{\lambda_{\max}}{\lambda_{\min}} \frac{1 + \sin \theta}{1 - \sin \theta}$ and $(\cdot)^+$ is the Moore-Penrose inverse. When \mathbf{A} is positive definite and $\mathbf{x} = \mathbf{y}$, i.e., $\mathbf{A}^+ = \mathbf{A}^{-1}$ and $\theta = 0$, the above inequality degenerates into the traditional form.

D Proof of Theorem 2

Proof According to Algorithm 3, we calculate the error as follows.

$$\begin{aligned} \mathbf{E}_{t+1} &= \mathbf{X}_{t+1} - \mathbf{X}_* \\ &= \mathcal{P}_r(\mathbf{Y}_t - \mu_t \nabla f(\mathbf{Y}_t)) - \mathbf{X}_* \\ &= \mathcal{P}_r(\mathbf{X}_* + \mathbf{Y}_t - \mathbf{X}_* - \mu_t \nabla f(\mathbf{Y}_t)) - \mathbf{X}_* \\ &= (\mathbf{Y}_t - \mathbf{X}_* - \mu_t \nabla f(\mathbf{Y}_t)) - P_{\mathbf{U}_*}^\perp (\mathbf{Y}_t - \mathbf{X}_* - \mu_t \nabla f(\mathbf{Y}_t)) P_{\mathbf{V}_*}^\perp + \mathcal{O}(\|\mathbf{Y}_t - \mathbf{X}_*\|_F^2). \end{aligned}$$

After vectorizing, we have

$$\begin{aligned} \mathbf{e}_{t+1} &= \underbrace{(\mathbf{I} - P_{\mathbf{V}_*}^\perp \otimes P_{\mathbf{U}_*}^\perp)(\mathbf{I} - \mu_t \boldsymbol{\Theta})}_{\mathbf{H}_t = \mathbf{H}(\mu_t)} \text{vec}(\mathbf{Y}_t - \mathbf{X}_*) + \mathcal{O}(\|\mathbf{Y}_t - \mathbf{X}_*\|_F^2) \\ &= (1 + \eta_t) \mathbf{H}_t \mathbf{e}_t - \eta_t \mathbf{H}_t \mathbf{e}_{t-1} + \mathcal{O}(\|\mathbf{e}_t\|_2^2). \end{aligned}$$

Stacking the errors of two adjacent iterations, we get the recursive form

$$\begin{pmatrix} \mathbf{e}_{t+1} \\ \mathbf{e}_t \end{pmatrix} = \underbrace{\begin{pmatrix} (1 + \eta_t) \mathbf{H}_t & -\eta_t \mathbf{H}_t \\ \mathbf{I} & \mathbf{0} \end{pmatrix}}_{\mathbf{T}} \begin{pmatrix} \mathbf{e}_t \\ \mathbf{e}_{t-1} \end{pmatrix}.$$

The convergence rate depends on the spectral radius $\rho(\mathbf{T})$ of $\mathbf{T} \in \mathbb{R}^{2n_1 n_2 \times 2n_1 n_2}$. According to the eigendecomposition in [34], \mathbf{T} is similar to the block diagonal matrix composed of the 2×2 matrix \mathbf{T}_j , i.e., $\mathbf{T} \sim \text{bldiag}(\mathbf{T}_1, \mathbf{T}_2, \dots, \mathbf{T}_{n_1 n_2})$, where each block $\mathbf{T}_j \in \mathbb{R}^{2 \times 2}$ is form

$$\mathbf{T}_j = \begin{pmatrix} (1 + \eta_t)(1 - \mu_t \lambda_j) & -\eta_t(1 - \mu_t \lambda_j) \\ 1 & 0 \end{pmatrix}.$$

where λ_j is the eigenvalue of matrix $(\mathbf{I} - P_{\mathbf{V}_*}^\perp \otimes P_{\mathbf{U}_*}^\perp) \boldsymbol{\Theta}$. Next, we aim to find the eigenvalues of the matrix \mathbf{T}_j using the characteristic polynomial.

$$r^2 - (1 + \eta_t)(1 - \mu_t \lambda_j)r + \eta_t(1 - \mu_t \lambda_j) = 0. \quad (31)$$

According to the quadratic formula, set the discriminant $\Delta(\lambda_j, \mu_t, \eta_t) = (1 + \eta_t)^2(1 - \mu_t \lambda_j)^2 - 4\eta_t(1 - \mu_t \lambda_j)$, then the solution to (31) is:

$$r^\pm(\lambda_j, \mu_t, \eta_t) = \frac{(1 + \eta_t)(1 - \mu_t \lambda_j) \pm \sqrt{\Delta(\lambda_j, \mu_t, \eta_t)}}{2}, \quad (32)$$

where the superscript $(\cdot)^\pm$ means addition or subtraction in numerator. For given \mathbf{T} with fixed (μ_t, η_t) , $\rho(\mathbf{T}) = \max_{\lambda_j} |r^\pm(\lambda_j, \mu_t, \eta_t)|$ is continuous and quasi-convex w.r.t. the eigenvalue λ_j [21, 18, 37]. Thus, the extremal value is attained on the boundary, i.e.

$$\rho(\mathbf{T}) = \max(|r^\pm(\lambda_{\max}, \mu_t, \eta_t)|, |r^\pm(\lambda_{\min}, \mu_t, \eta_t)|). \quad (33)$$

As a whole, $\rho(\mathbf{T})$ is determined by the maximum modulus of the roots of (33). We denote that surfaces Π_1 and Π_2 correspond to λ_{\min} and λ_{\max} , respectively.

Below we show how to determine the minimum spectral radius and corresponding parameters. Back to (32), $|r^\pm(\lambda_j, \mu_t, \eta_t)| \geq |(1 + \eta_t)(1 - \mu_t \lambda_j)|/2$ takes the equal if and only if $\Delta(\lambda_j, \mu_t, \eta_t) = 0$. In this case, we can get a relationship of the parameter (μ_t, η_t)

$$\eta_t^- = \frac{1 - \sqrt{\mu_t \lambda_j}}{1 + \sqrt{\mu_t \lambda_j}}, \eta_t^+ = \frac{1 + \sqrt{\mu_t \lambda_j}}{1 - \sqrt{\mu_t \lambda_j}}. \quad (34)$$

Obviously, $0 < \eta_t^- < 1 < \eta_t^+$. Given μ_t , there are three cases for η_t .

- (32) with $\eta_t \in (0, \eta_t^-) \cup (\eta_t^+, \infty)$ has two different solutions.
- (32) with $\eta_t = \eta_t^\pm$ has a single solution.
- (32) with $\eta_t \in (\eta_t^-, \eta_t^+)$ has conjugate complex solutions.

If $\eta_t \in [\eta_t^+, \infty)$, $r^\pm(\lambda_j, \mu_t, \eta_t^+) \geq |(1 + \eta_t^+)(1 - \mu_t \lambda_j)|/2 = 1 + \sqrt{\mu_t \lambda_j} > 1$, and $\rho(\mathbf{T}) > 1$ is obtained from (33). Conversely, when $\eta_t = \eta_t^-$, $r^\pm(\lambda_j, \mu_t, \eta_t^-) = |(1 + \eta_t^-)(1 - \mu_t \lambda_j)|/2 = 1 - \sqrt{\mu_t \lambda_j} < 1$. This is also why the parameter is selected as $0 < \eta \leq 1$ in practice. When $\eta_t \in (\eta_t^-, \eta_t^+)$, $\rho(\mathbf{T}) = \max_{\lambda_j} \sqrt{\eta_t(1 - \mu_t \lambda_j)}$ monotonically increases w.r.t. η_t and monotonically decreases w.r.t. μ_t . We can draw the geometric properties of $\rho(\mathbf{T})$ w.r.t. (μ_t, η_t) , and condition $\Delta(\lambda_j, \mu_t, \eta_t^-) = 0$ helps to find the theoretical lower bound of $\rho(\mathbf{T})$. The optimal parameter pair (μ_b, η_b) is the intersection of $r^\pm(\lambda_{\min}, \mu_b, \eta_b)$ in the curve $\eta_t^- = \frac{1 - \sqrt{\mu_t \lambda_j}}{1 + \sqrt{\mu_t \lambda_j}}$ and the surface Π_2 , i.e., $|r^-(\lambda_{\max}, \mu_t, \eta_t)|$. So it satisfies the following equation

$$(1 + \eta_b)(1 - \mu_b \lambda_{\min}) = -(1 + \eta_b)(1 - \mu_b \lambda_{\max}^2) + \sqrt{(1 + \eta_b)^2(1 - \mu_b \lambda_{\max}^2)^2 - 4\eta_b(1 - \mu_b \lambda_{\max}^2)}.$$

Bringing in $\eta_b = \frac{1 - \sqrt{\mu_b \lambda_{\min}}}{1 + \sqrt{\mu_b \lambda_{\min}}}$, it is not difficult for us to get optimal convergence result $\mu_b = \frac{4}{\lambda_{\min} + 3\lambda_{\max}}$ and $\rho_{\text{opt}}(\mathbf{T}) = 1 - \sqrt{\frac{4\lambda_{\min}}{\lambda_{\min} + 3\lambda_{\max}}}$ in (18). Also, for $\eta_t < 1$, the intersection of Π_1 and Π_2 can be calculated according to monotonicity

$$r^+(\lambda_{\min}, \mu_t, \eta_t) = -r^-(\lambda_{\max}, \mu_t, \eta_t).$$

If $\eta_t = 0$, it simplifies to $\mu_t = 2/(\lambda_{\min} + \lambda_{\max}) = \mu_\dagger$ in (11). Due to momentum, the optimal stepsizes satisfy $\mu_b < \mu_\dagger$. In fact, we bring $\eta_t = 0$ to get $\mathbf{e}_t = \mathbf{H}\mathbf{e}_{t-1} + \mathcal{O}(\|\mathbf{e}_{t-1}\|_2^2)$, which is consistent with the non-accelerated iteration. Conversely, if $\mu_t \geq \mu_\dagger$, then $\eta_t = 0$ is a good parameter choice, which means NAG degenerates to Grad. When $\eta_t \neq 0$, we have

$$\eta_t \mu_t^2 (\lambda_{\max} - \lambda_{\min})^2 + 2(1 + \eta_t)^2 (1 - \mu_t \lambda_{\max})(1 - \mu_t \lambda_{\min})(2 - \mu_t(\lambda_{\min} + \lambda_{\max})) = 0.$$

Despite the complex form, we use symbolic computing tools to solve when $\mu_t \in (\mu_b, \mu_\dagger)$

$$\begin{aligned} \eta_{t\otimes} = & [(-4\lambda_{\min}^2 \lambda_{\max} \mu_t^3 + 5\lambda_{\min}^2 \mu_t^2 - 4\lambda_{\min} \lambda_{\max}^2 \mu_t^3 + 14\lambda_{\min} \lambda_{\max} \mu_t^2 - 12\lambda_{\min} \mu_t + 5\lambda_{\max}^2 \mu_t^2 - 12\lambda_{\max} \mu_t + 8) \\ & - \sqrt{\mu_t^2 (-\lambda_{\max} - \lambda_{\min})^2 (8\lambda_{\min}^2 \lambda_{\max} \mu_t^3 - 9\lambda_{\min}^2 \mu_t^2 + 8\lambda_{\min} \lambda_{\max}^2 \mu_t^3 - 30\lambda_{\min} \mu_t^2 + 24\lambda_{\min} \mu_t - 9\lambda_{\max}^2 \mu_t^2 + 24\lambda_{\max} \mu_t - 16)} \\ & / (4(\lambda_{\min} \mu_t - 1)(\lambda_{\max} \mu_t - 1)(\lambda_{\min} \mu_t + \lambda_{\max} \mu_t - 2)). \end{aligned}$$

We analyze the spectral radius of \mathbf{T} in (33) w.r.t. pair (μ_t, η_t) by case. \square

E Proof in Sect. 4

E.1 Proof of Lemma 3

Proof The first one obviously holds according to Lemma 1. From (25), we have

$$\begin{aligned}
\mathcal{R}_{\mathbf{X}}^{\text{orth}}(\mathbf{N}) &= (\mathbf{X} + \mathbf{N})\mathbf{V}_{\mathbf{X}}(\boldsymbol{\Sigma}_{\mathbf{X}} + \mathbf{U}_{\mathbf{X}}^{\top}\mathbf{N}\mathbf{V}_{\mathbf{X}})^{-1}\mathbf{U}_{\mathbf{X}}^{\top}(\mathbf{X} + \mathbf{N}) \\
&\stackrel{(a)}{=} (\mathbf{X} + \mathbf{N})\mathbf{V}_{\mathbf{X}}(\boldsymbol{\Sigma}_{\mathbf{X}}^{-1} - \boldsymbol{\Sigma}_{\mathbf{X}}^{-1}\mathbf{U}_{\mathbf{X}}^{\top}\mathbf{N}\mathbf{V}_{\mathbf{X}}\boldsymbol{\Sigma}_{\mathbf{X}}^{-1})\mathbf{U}_{\mathbf{X}}^{\top}(\mathbf{X} + \mathbf{N}) + \mathcal{O}(\|\mathbf{N}\|_F^2) \\
&= (\mathbf{X} + \mathbf{N})(\mathbf{V}_{\mathbf{X}}\boldsymbol{\Sigma}_{\mathbf{X}}^{-1}\mathbf{U}_{\mathbf{X}}^{\top} - \mathbf{V}_{\mathbf{X}}\boldsymbol{\Sigma}_{\mathbf{X}}^{-1}\mathbf{U}_{\mathbf{X}}^{\top}\mathbf{N}\mathbf{V}_{\mathbf{X}}\boldsymbol{\Sigma}_{\mathbf{X}}^{-1}\mathbf{U}_{\mathbf{X}}^{\top})(\mathbf{X} + \mathbf{N}) + \mathcal{O}(\|\mathbf{N}\|_F^2) \\
&= (\mathbf{X} + \mathbf{N})(\mathbf{X}^{-\top} - \mathbf{X}^{-\top}\mathbf{N}\mathbf{X}^{-\top})(\mathbf{X} + \mathbf{N}) + \mathcal{O}(\|\mathbf{N}\|_F^2) \\
&\stackrel{(b)}{=} \mathbf{X}\mathbf{X}^{-\top}\mathbf{X} + \mathbf{N}\mathbf{X}^{-\top}\mathbf{X} + \mathbf{X}\mathbf{X}^{-\top}\mathbf{N} - \mathbf{X}\mathbf{X}^{-\top}\mathbf{N}\mathbf{X}^{-\top}\mathbf{X} + \mathcal{O}(\|\mathbf{N}\|_F^2) \\
&\stackrel{(c)}{=} \mathbf{X} + P_{\mathbf{U}_{\mathbf{X}}}\mathbf{N} + \mathbf{N}P_{\mathbf{V}_{\mathbf{X}}} - P_{\mathbf{U}_{\mathbf{X}}}\mathbf{N}P_{\mathbf{V}_{\mathbf{X}}} + \mathcal{O}(\|\mathbf{N}\|_F^2) \\
&= \mathbf{X} + \mathbf{N} - P_{\mathbf{U}_{\mathbf{X}}}^{\perp}\mathbf{N}P_{\mathbf{V}_{\mathbf{X}}}^{\perp} + \mathcal{O}(\|\mathbf{N}\|_F^2) \\
&= \mathcal{P}_{\mathbb{T}_{\mathbf{X}}}(\mathbf{X} + \mathbf{N}) + \mathcal{O}(\|\mathbf{N}\|_F^2),
\end{aligned}$$

where (a) is the perturbation analysis of matrix inverse. As long as $\|\mathbf{A}^{-1}\mathbf{B}\| < 1$ or $\|\mathbf{B}\mathbf{A}^{-1}\| < 1$ holds, the Taylor expansion of the inverse of the matrix sum is as follows

$$\begin{aligned}
(\mathbf{A} + \mathbf{B})^{-1} &= \mathbf{A}^{-1} - \mathbf{A}^{-1}\mathbf{B}\mathbf{A}^{-1} + \mathbf{A}^{-1}(\mathbf{B}\mathbf{A}^{-1})^2 - \mathbf{A}^{-1}(\mathbf{B}\mathbf{A}^{-1})^3 + \dots \\
&= \mathbf{A}^{-1} - \mathbf{A}^{-1}\mathbf{B}\mathbf{A}^{-1} + \mathcal{O}(\|\mathbf{B}\|_F^2).
\end{aligned}$$

Using the norm inequality $\|\mathbf{A}\mathbf{B}\| \leq \|\mathbf{A}\|\|\mathbf{B}\|$, combined with the condition $\|\mathbf{N}\| \leq \|\mathbf{N}\|_F < \sigma_r(\mathbf{X})/2$, it can be judged that the inverse matrix condition holds.

$$\|\boldsymbol{\Sigma}_{\mathbf{X}}^{-1}(\mathbf{U}_{\mathbf{X}}^{\top}\mathbf{N}\mathbf{V}_{\mathbf{X}})\| \leq \frac{\|\mathbf{U}_{\mathbf{X}}^{\top}\mathbf{N}\mathbf{V}_{\mathbf{X}}\|}{\|\boldsymbol{\Sigma}_{\mathbf{X}}\|} \leq \frac{\|\mathbf{N}\|}{\sigma_r(\mathbf{X})} < 1.$$

(b) merges the product of multiple \mathbf{N} into higher-order terms. (c) uses the SVD of \mathbf{X} to get

$$\begin{aligned}
\mathbf{X}\mathbf{X}^{-\top} &= \mathbf{U}_{\mathbf{X}}\boldsymbol{\Sigma}_{\mathbf{X}}\mathbf{V}_{\mathbf{X}}^{\top}\mathbf{V}_{\mathbf{X}}\boldsymbol{\Sigma}_{\mathbf{X}}^{-1}\mathbf{U}_{\mathbf{X}}^{\top} = \mathbf{U}_{\mathbf{X}}\mathbf{U}_{\mathbf{X}}^{\top} = P_{\mathbf{U}_{\mathbf{X}}}, \\
\mathbf{X}^{-\top}\mathbf{X} &= \mathbf{V}_{\mathbf{X}}\boldsymbol{\Sigma}_{\mathbf{X}}^{-1}\mathbf{U}_{\mathbf{X}}^{\top}\mathbf{U}_{\mathbf{X}}\boldsymbol{\Sigma}_{\mathbf{X}}\mathbf{V}_{\mathbf{X}}^{\top} = \mathbf{V}_{\mathbf{X}}\mathbf{V}_{\mathbf{X}}^{\top} = P_{\mathbf{V}_{\mathbf{X}}}, \\
\mathbf{X}\mathbf{X}^{-\top}\mathbf{X} &= P_{\mathbf{U}_{\mathbf{X}}}\mathbf{U}_{\mathbf{X}}\boldsymbol{\Sigma}_{\mathbf{X}}\mathbf{V}_{\mathbf{X}}^{\top} = \mathbf{U}_{\mathbf{X}}\boldsymbol{\Sigma}_{\mathbf{X}}\mathbf{V}_{\mathbf{X}}^{\top} = \mathbf{X}.
\end{aligned}$$

□

E.2 Convergence for Algorithm 4

Proof According to Algorithm 4, we have

$$\begin{aligned}
\mathbf{E}_{t+1} &= \mathcal{R}_{\mathbf{X}_t}(-\mu_t \text{grad}f(\mathbf{X}_t)) - \mathbf{X}_{\star} \\
&\stackrel{(a)}{=} \mathcal{P}_{\mathbb{T}_{\mathbf{X}_t}\mathbb{M}_r}(\mathbf{X}_t - \mu_t \nabla f(\mathbf{X}_t)) - \mathbf{X}_{\star} + \mathcal{O}(\|\mathbf{E}_t\|_F^2) \\
&\stackrel{(b)}{=} (\mathbf{E}_t - \mu_t \nabla f(\mathbf{X}_t)) - P_{\mathbf{U}_t}^{\perp}(\mathbf{E}_t - \mu_t \nabla f(\mathbf{X}_t))P_{\mathbf{V}_t}^{\perp} + \mathcal{O}(\|\mathbf{E}_t\|_F^2) \\
&\stackrel{(c)}{=} (\mathbf{E}_t - \mu_t \nabla f(\mathbf{X}_t)) - P_{\mathbf{U}_{\star}}^{\perp}(\mathbf{E}_t - \mu_t \nabla f(\mathbf{X}_t))P_{\mathbf{V}_{\star}}^{\perp} + \mathcal{O}(\|\mathbf{E}_t\|_F^2),
\end{aligned}$$

where (a) uses Lemma 3, (b) is based on the tangent space projection in (22), and (c) uses the subspace perturbation in Lemma 5, and replaces the subspace $\mathcal{P}_{\mathbb{T}_{\mathbf{X}_t \mathbb{M}_r}}$ with $\mathcal{P}_{\mathbb{T}_{\mathbf{X}_\star \mathbb{M}_r}}$.

$$\begin{aligned} \|P_{\tilde{\mathbf{U}}_t}^\perp \mathbf{A} P_{\tilde{\mathbf{V}}_t}^\perp - P_{\tilde{\mathbf{U}}_\star}^\perp \mathbf{A} P_{\tilde{\mathbf{V}}_\star}^\perp\| &= \|P_{\tilde{\mathbf{U}}_t}^\perp \mathbf{A} P_{\tilde{\mathbf{V}}_t}^\perp - P_{\tilde{\mathbf{U}}_t}^\perp \mathbf{A} P_{\tilde{\mathbf{V}}_\star}^\perp + P_{\tilde{\mathbf{U}}_t}^\perp \mathbf{A} P_{\tilde{\mathbf{V}}_\star}^\perp - P_{\tilde{\mathbf{U}}_\star}^\perp \mathbf{A} P_{\tilde{\mathbf{V}}_\star}^\perp\| \\ &\leq \|P_{\tilde{\mathbf{U}}_t}^\perp \mathbf{A} P_{\tilde{\mathbf{V}}_t}^\perp - P_{\tilde{\mathbf{U}}_t}^\perp \mathbf{A} P_{\tilde{\mathbf{V}}_\star}^\perp\| + \|P_{\tilde{\mathbf{U}}_t}^\perp \mathbf{A} P_{\tilde{\mathbf{V}}_\star}^\perp - P_{\tilde{\mathbf{U}}_\star}^\perp \mathbf{A} P_{\tilde{\mathbf{V}}_\star}^\perp\| \\ &\leq \|P_{\tilde{\mathbf{U}}_t}^\perp\| \|\mathbf{A}\| \|P_{\tilde{\mathbf{V}}_t}^\perp - P_{\tilde{\mathbf{V}}_\star}^\perp\| + \|P_{\tilde{\mathbf{U}}_t}^\perp - P_{\tilde{\mathbf{U}}_\star}^\perp\| \|\mathbf{A}\| \|P_{\tilde{\mathbf{V}}_\star}^\perp\| \\ &= \mathcal{O}(\|\mathbf{E}_t\|_F^2), \end{aligned}$$

The subsequent proof is consistent with the proof of Theorem 1 in Appendix B. \square

E.3 Convergence for Algorithm 5

Proof The proof is divided into three steps to analyse \mathbf{X}_{t-1} , \mathbf{Y}_t and \mathbf{X}_{t+1} , respectively.

Step 1: Calculate the orthographic retraction of \mathbf{X}_{t-1} and the inverse matrix.

$$\begin{aligned} \text{inv}\mathcal{R}_{\mathbf{X}_t}^{\text{orth}}(\mathbf{X}_{t-1}) &= \mathcal{P}_{\mathbb{T}_{\mathbf{X}_t \mathbb{M}_r}}(\mathbf{X}_{t-1} - \mathbf{X}_t) \\ &= \mathcal{P}_{\mathbb{T}_{\mathbf{X}_t \mathbb{M}_r}}(\mathbf{X}_{t-1}) - \mathbf{X}_t \\ &= \mathcal{P}_{\mathbb{T}_{\mathbf{X}_\star \mathbb{M}_r}}(\mathbf{X}_{t-1}) - \mathbf{X}_t + \mathcal{O}(\|\mathbf{E}_t\|_F^2) \\ &= \mathbf{X}_{t-1} - \mathbf{X}_t + \mathcal{O}(\|\mathbf{E}_t\|_F^2 + \|\mathbf{E}_{t-1}\|_F^2). \end{aligned}$$

It gives an approximation of \mathbf{X}_{t-1} on the tangent space $\mathbb{T}_{\mathbf{X}_t \mathbb{M}_r}$.

Step 2: Similar to Appendix D, we calculate the residual of \mathbf{Y}_t

$$\begin{aligned} \mathbf{Y}_t - \mathbf{X}_\star &= \mathcal{R}_{\mathbf{X}_t}^{\text{orth}}(-\eta_t \text{inv}\mathcal{R}_{\mathbf{X}_t}^{\text{orth}}(\mathbf{X}_{t-1})) - \mathbf{X}_\star \\ &= \mathcal{P}_{\mathbb{T}_{\mathbf{X}_t \mathbb{M}_r}}(\mathbf{X}_t - \eta_t \text{inv}\mathcal{R}_{\mathbf{X}_t}^{\text{orth}}(\mathbf{X}_{t-1})) - \mathbf{X}_\star + \mathcal{O}(\|\mathbf{E}_t\|_F^2) \\ &= \mathbf{X}_t - \eta_t \text{inv}\mathcal{R}_{\mathbf{X}_t}^{\text{orth}}(\mathbf{X}_{t-1}) - \mathbf{X}_\star + \mathcal{O}(\|\mathbf{E}_t\|_F^2) \\ &= \mathbf{X}_t - \mathbf{X}_\star + \eta_t (\mathbf{X}_t - \mathbf{X}_{t-1}) + \mathcal{O}(\|\mathbf{E}_t\|_F^2 + \|\mathbf{E}_{t-1}\|_F^2) \\ &= \mathbf{E}_t + \eta_t (\mathbf{E}_t - \mathbf{E}_{t-1}) + \mathcal{O}(\|\mathbf{E}_t\|_F^2 + \|\mathbf{E}_{t-1}\|_F^2). \end{aligned}$$

It also satisfies the linear extrapolation in Euclidean space.

Step 3: Compute $\mathbf{X}_{t+1} - \mathbf{X}_\star$ to get the recursive form

$$\begin{aligned} \mathbf{E}_{t+1} &= \mathbf{X}_{t+1} - \mathbf{X}_\star \\ &= \mathcal{R}_{\mathbf{Y}_t}^{\text{orth}}(-\mu_t \text{grad}f(\mathbf{Y}_t)) - \mathbf{X}_\star \\ &= \mathcal{P}_{\mathbb{T}_{\mathbf{Y}_t \mathbb{M}_r}}(\mathbf{Y}_t - \mu_t \nabla f(\mathbf{Y}_t)) - \mathbf{X}_\star + \mathcal{O}(\|\mathbf{Y}_t - \mathbf{X}_\star\|_F^2) \\ &= \mathcal{P}_{\mathbb{T}_{\mathbf{X}_\star \mathbb{M}_r}}(\mathbf{Y}_t - \mu_t \nabla f(\mathbf{Y}_t)) - \mathbf{X}_\star + \mathcal{O}(\|\mathbf{Y}_t - \mathbf{X}_\star\|_F^2) \\ &= (\mathbf{Y}_t - \mathbf{X}_\star - \mu_t \nabla f(\mathbf{Y}_t)) - P_{\tilde{\mathbf{U}}_\star}^\perp (\mathbf{Y}_t - \mathbf{X}_\star - \mu_t \nabla f(\mathbf{Y}_t)) P_{\tilde{\mathbf{V}}_\star}^\perp + \mathcal{O}(\|\mathbf{Y}_t - \mathbf{X}_\star\|_F^2). \end{aligned}$$

The subsequent proof is consistent with proof of Theorem 2 in Appendix D. \square

E.4 Proof of Restart Condition Equivalence in (28)

Proof When condition (8) hold, we have

$$\begin{aligned}
\langle \nabla f(\mathbf{Y}_{t-1}), \mathbf{X}_t - \mathbf{X}_{t-1} \rangle &= \langle \text{grad } f(\mathbf{Y}_{t-1}) + \nabla f(\mathbf{Y}_{t-1}) - \text{grad } f(\mathbf{Y}_{t-1}), \mathbf{X}_t - \mathbf{X}_{t-1} \rangle \\
&\stackrel{(a)}{=} \langle \text{grad } f(\mathbf{Y}_{t-1}), \text{inv}\mathcal{R}_{\mathbf{Y}_{t-1}}^{\text{orth}}(\mathbf{X}_t) - \text{inv}\mathcal{R}_{\mathbf{Y}_{t-1}}^{\text{orth}}(\mathbf{X}_{t-1}) \rangle \\
&\quad + \langle \nabla f(\mathbf{Y}_{t-1}) - \text{grad } f(\mathbf{Y}_t), \mathbf{X}_t - \text{inv}\mathcal{R}_{\mathbf{Y}_{t-1}}^{\text{orth}}(\mathbf{X}_t) \rangle \\
&\quad - \langle \nabla f(\mathbf{Y}_{t-1}) - \text{grad } f(\mathbf{Y}_t), \mathbf{X}_{t-1} - \text{inv}\mathcal{R}_{\mathbf{Y}_{t-1}}^{\text{orth}}(\mathbf{X}_{t-1}) \rangle \\
&\stackrel{(b)}{\approx} \langle \text{grad } f(\mathbf{Y}_{t-1}), \text{inv}\mathcal{R}_{\mathbf{Y}_{t-1}}^{\text{orth}}(\mathbf{X}_t) - \text{inv}\mathcal{R}_{\mathbf{Y}_{t-1}}^{\text{orth}}(\mathbf{X}_{t-1}) \rangle,
\end{aligned}$$

where (a) uses the orthogonal relationship of the Riemannian gradient and tangent space. Based on the first-order expansion, we appropriately omit the higher-order terms in (a) to obtain the approximate relationship (b), which will not change the sign before and after the approximation. As mentioned in step 2 in Appendix E.3, $\nabla f(\mathbf{Y}_{t-1}) = \Theta \text{vec}(\mathbf{Y}_{t-1} - \mathbf{X}_*)$ and $\text{grad } f(\mathbf{Y}_{t-1})$ both are first order w.r.t. the residual. According to Lemma 3, $\mathbf{X}_t - \text{inv}\mathcal{R}_{\mathbf{Y}_{t-1}}^{\text{orth}}(\mathbf{X}_t)$ and $\mathbf{X}_{t-1} - \text{inv}\mathcal{R}_{\mathbf{Y}_{t-1}}^{\text{orth}}(\mathbf{X}_{t-1})$ are second order. So the last two terms of (a) are third order, while the remaining inner product is second order. \square

References

1. Absil, P.A., Malick, J.: Projection-like retractions on matrix manifolds. *SIAM J. Optim.* **22**(1), 135–158 (2012)
2. Absil, P.A., Oseledets, I.V.: Low-rank retractions: a survey and new results. *Comput. Optim. Appl.* **62**(1), 5–29 (2015)
3. Ahn, K., Sra, S.: From Nesterov’s estimate sequence to Riemannian acceleration. In: *Conference on Learning Theory*, pp. 84–118. PMLR (2020)
4. Boumal, N.: *An introduction to optimization on smooth manifolds*. Cambridge University Press (2023)
5. Cai, J.F., Wei, K.: Exploiting the structure effectively and efficiently in low-rank matrix recovery. In: *Handbook of Numerical Analysis*, vol. 19, pp. 21–51. Elsevier (2018)
6. Chen, Y., Chi, Y.: Harnessing structures in big data via guaranteed low-rank matrix estimation: Recent theory and fast algorithms via convex and nonconvex optimization. *IEEE Signal Process Mag.* **35**(4), 14–31 (2018)
7. Chen, Y., Chi, Y., Fan, J., Ma, C.: Gradient descent with random initialization: Fast global convergence for nonconvex phase retrieval. *Mathematical Programming* **176**, 5–37 (2019)
8. Chen, Y., Chi, Y., Fan, J., Ma, C., et al.: Spectral methods for data science: A statistical perspective. *Found. Trends Mach. Learn.* **14**(5), 566–806 (2021)
9. Chi, Y., Lu, Y.M., Chen, Y.: Nonconvex optimization meets low-rank matrix factorization: An overview. *IEEE Trans. Signal Process.* **67**(20), 5239–5269 (2019)
10. Chunikhina, E., Raich, R., Nguyen, T.: Performance analysis for matrix completion via iterative hard-thresholded SVD. In: *2014 IEEE Workshop on Statistical Signal Processing (SSP)*, pp. 392–395. IEEE (2014)
11. Davenport, M.A., Romberg, J.: An overview of low-rank matrix recovery from incomplete observations. *IEEE J. Sel. Top. Signal Process.* **10**(4), 608–622 (2016)
12. Duruisseaux, V., Leok, M.: A variational formulation of accelerated optimization on Riemannian manifolds. *SIAM J. Math. Data Sci.* **4**(2), 649–674 (2022)
13. Gonzaga, C.C., Schneider, R.M.: On the steepest descent algorithm for quadratic functions. *Comput. Optim. Appl.* **63**, 523–542 (2016)
14. Huang, J., Zhou, J.: A direct proof and a generalization for a Kantorovich type inequality. *Linear Algebra Appl.* **397**, 185–192 (2005)

15. Huang, W., Wei, K.: An extension of fast iterative shrinkage-thresholding algorithm to Riemannian optimization for sparse principal component analysis. *Numer. Linear Algebra Appl.* **29**(1), e2409 (2022)
16. Huang, Y., Dai, Y.H., Liu, X.W., Zhang, H.: On the asymptotic convergence and acceleration of gradient methods. *J. Sci. Comput.* **90**, 1–29 (2022)
17. Jain, P., Meka, R., Dhillon, I.: Guaranteed rank minimization via singular value projection. *Advances in Neural Information Processing Systems* **23** (2010)
18. Kim, D., Fessler, J.A.: Adaptive restart of the optimized gradient method for convex optimization. *J. Optim. Theory Appl.* **178**(1), 240–263 (2018)
19. Kim, J., Yang, I.: Nesterov acceleration for Riemannian optimization. *arXiv preprint arXiv:2202.02036* (2022)
20. Kyrillidis, A., Cevher, V.: Matrix recipes for hard thresholding methods. *J. Math. Imaging Vision* **48**, 235–265 (2014)
21. Lessard, L., Recht, B., Packard, A.: Analysis and design of optimization algorithms via integral quadratic constraints. *SIAM J. Optim.* **26**(1), 57–95 (2016)
22. Li, H., Fang, C., Lin, Z.: Accelerated first-order optimization algorithms for machine learning. *Proc. IEEE* **108**(11), 2067–2082 (2020)
23. Li, H., Lin, Z.: Accelerated alternating direction method of multipliers: An optimal $o(1/k)$ nonergodic analysis. *J. Sci. Comput.* **79**, 671–699 (2019)
24. Liang, J., Fadili, J., Peyré, G.: Activity identification and local linear convergence of forward–backward-type methods. *SIAM J. Optim.* **27**(1), 408–437 (2017)
25. Liang, J., Luo, T., Schonlieb, C.B.: Improving “fast iterative shrinkage-thresholding algorithm”: Faster, smarter, and greedier. *SIAM J. Sci. Comput.* **44**(3), A1069–A1091 (2022)
26. Luenberger, D.G., Ye, Y.: *Linear and Nonlinear Programming*, vol. 228. Springer Nature (2021)
27. Nesterov, Y.E.: A method of solving a convex programming problem with convergence rate $o(k^{-2})$. In: *Doklady Akademii Nauk*, vol. 269, pp. 543–547. Russian Academy of Sciences (1983)
28. O’donoghue, B., Candes, E.: Adaptive restart for accelerated gradient schemes. *Found. Comput. Math.* **15**, 715–732 (2015)
29. Park, J.: Accelerated additive schwarz methods for convex optimization with adaptive restart. *J. Sci. Comput.* **89**(3), 58 (2021)
30. Polyak, B.T.: Some methods of speeding up the convergence of iteration methods. *Ussr computational mathematics and mathematical physics* **4**(5), 1–17 (1964)
31. Tanner, J., Wei, K.: Normalized iterative hard thresholding for matrix completion. *SIAM Journal on Scientific Computing* **35**(5), S104–S125 (2013)
32. Tong, T., Ma, C., Chi, Y.: Accelerating ill-conditioned low-rank matrix estimation via scaled gradient descent. *J. Mach. Learn. Res.* **22**(1), 6639–6701 (2021)
33. Vandereycken, B.: Low-rank matrix completion by Riemannian optimization. *SIAM J. Optim.* **23**(2), 1214–1236 (2013)
34. Vu, T., Raich, R.: Accelerating iterative hard thresholding for low-rank matrix completion via adaptive restart. In: *2019 IEEE International Conference on Acoustics, Speech and Signal Processing (ICASSP)*, pp. 2917–2921. IEEE (2019)
35. Vu, T., Raich, R.: On local convergence of iterative hard thresholding for matrix completion. *arXiv preprint arXiv:2112.14733* (2021)
36. Vu, T., Raich, R.: On asymptotic linear convergence of projected gradient descent for constrained least squares. *IEEE Trans. Signal Process.* **70**, 4061–4076 (2022)
37. Wang, D., He, Y., De Sterck, H.: On the asymptotic linear convergence speed of anderson acceleration applied to ADMM. *J. Sci. Comput.* **88**(2), 38 (2021)
38. Wang, H., Cai, J.F., Wang, T., Wei, K.: Fast Cadzow’s algorithm and a gradient variant. *J. Sci. Comput.* **88**(2), 41 (2021)
39. Wang, R., Zhang, C., Wang, L., Shao, Y.: A stochastic Nesterov’s smoothing accelerated method for general nonsmooth constrained stochastic composite convex optimization. *J. Sci. Comput.* **93**(2), 52 (2022)
40. Wei, K., Cai, J.F., Chan, T.F., Leung, S.: Guarantees of Riemannian optimization for low rank matrix recovery. *SIAM J. Matrix Anal. Appl.* **37**(3), 1198–1222 (2016)
41. Wei, K., Cai, J.F., Chan, T.F., Leung, S.: Guarantees of Riemannian optimization for low rank matrix completion. *Inverse Problems and Imaging* **14**(2), 233–265 (2020)

-
42. Wibisono, A., Wilson, A.C., Jordan, M.I.: A variational perspective on accelerated methods in optimization. *Proc. Natl. Acad. Sci.* **113**(47), E7351–E7358 (2016)
 43. Zhang, H., Sra, S.: Towards Riemannian accelerated gradient methods. arXiv preprint arXiv:1806.02812 (2018)
 44. Zhang, T., Yang, Y.: Robust PCA by manifold optimization. *J Mach Learn Res* **19**(1), 3101–3139 (2018)